4-2018

Diatomaceous Solar Cells

Jesse Granger

Diatomaceous Solar Cells

A thesis submitted in partial fulfillment of the requirements for the degree of Bachelor of Science with Honors in Interdisciplinary Biophysics from the College of William and Mary in Virginia

By

Jesse N. Granger

Honors
Accepted for (Honors, Not Honors)

Advisor: Prof. William Cooke

Prof. Dennis Manos

Prof. Kristin Wustholz

Prof. Irina Novikova

Williamsburg, Virginia

May 2018

Contents

List of Figures

Figure 34: Edge of TiO_2 coated slide taken on PHENOM

Figure 35: P3HT coated FTO on Phenom. 75 degree angle

Figure 36: Gold Sputter Coater Calibration, measured by masking slides and sputtering for different increments, then measuring the thickness using a DEKTAK

Figure 37: An example of a complete assembly. Top image shows the back of the cell, with the gold back-electrode. Bottom image shows the top of the cell where light would enter. Note: The streaks came from the spin coater on the back side of the glass, and are not due to inhomogeneity in the layer

Figure 38: Top: TiO_2 layer against an N-doped silicon wafer showing clear rectification in the negative direction. Middle: PEDOT:PSS against a p-doped silicon wafer showing clear rectification in the positive direction. Bottom: TiO_2 vs PEDOT:PSS not showing any significant rectification

List of Tables

Abstract

An experiment was conducted at the college of William and Mary to explore the ability of wild type diatoms to enhance the abilities of a Dye-Sensitized Solar Cell (DSSC). The goal was to see if the efficiency of a solar cell could be enhanced by the addition of wild-type diatoms in the active layer of the cell, and if there was any notable advantage to using diatoms where the frustule material had been altered. For this purpose, diatoms were cleaned using near-boiling baths of hydrogen peroxide and then coated in Titanium Dioxide using a peptide-mediated deposition [1]. Diatoms were tested under the TOF-SIMS and found to have an average atomic count Ti:Si ratio of 2.5 (range of .54—4.6) Ti/Si. DSSCs were then assembled: Two with no diatoms, two with uncoated diatoms, and two with coated diatoms. The cells without diatoms were found to have an efficiency of 1.78% ± .23%, the uncoated diatoms cells were found to have an efficiency of 1.11% ± .57%, and the coated diatoms cells were found to have an efficiency of .6311% ± .04%. These results do not show any indication that the diatoms have increased the efficiency of the solar cells at this time, nor is there any evidence that altering the frustrule material is advantageous for solar cell efficiency. These results may be due to problems in the consistency of our assembly process, and further research should focus on developing a method for depositing a reliable thickness for the TiO_2 layer, and solving the saturation problem currently seen in our cells.

Chapter 1: Introduction

1.1 The Goal of the Experiment

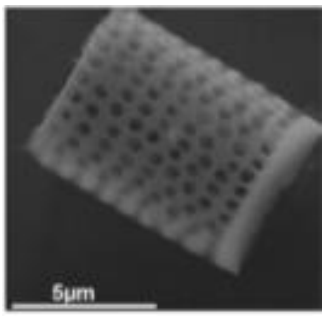

Figure 1: A Diatom Frustule. [5]

Solar-power promises to be one of the most ideal sources of sustainable, environmentally-friendly energy; however, our current solar-cell devices are expensive, inefficient, and often use toxic substrates in their production. Solar cells are still not a feasible addition for most households because of their cost. Meanwhile, floating within almost every body of water on the planet, the diatom has spent millennia fine-tuning its own ability to capture solar energy.

The diatoms are a species of single-cellular photosynthetic algae which are abundant in most bodies of water. Their exoskeleton, known as a frustule, is made of amorphous bio-silica [3]. An example of a frustule can be seen in figure 1, note the hierarchical, 3-D pore structure that makes up the diatom's cell wall. The frustule's mechanical strength, complex 3D structure, multilevel nanopores, and large surface area make them a potentially novel material for integration into solar cells [4]. In addition, the frustule has unique optical properties. Although diatoms appear in a variety of different shapes (See Jeffryes et. al [4] for an exhaustive review of diatom anatomy), the frustrule of all diatoms have pores at the nanoscale making them ideal for photovoltaic system [3][4][9]. This sophisticated, porous structure of the frustrule has also been shown to couple incoming light into distinct photonic bandgaps and thus acts as a photonic crystal [4][6][9]. Photonic crystals act as integrated reflectors and thus could increase the amount of energy gained from incoming light in a solar cell. Because these low-cost frustules have so many features that are desired in a solar cell, it has been hypothesized that the diatom could revolutionize the ways in which photovoltaic energy devices are manufactured [4][9]. Several researchers have shown that diatoms can be used for electrochemical use [3][4], and others have incorporated them into DSSCs using ruthenium-based dye and platinum back electrodes [2][3]. Some researchers though have claimed that only frustules whose composition has been altered to be more compatible with a photovoltaic system will be applicable in solar cell application [2][5], while others have submitted evidence that suggests the unaltered frustule should be sufficient [3]. My research explores the feasibility of using wild diatoms (multiple species harvested from a river) to increase the efficiency of a low-cost 3rd generation solar cell, and whether or not there is evidence that converting the surface material of the frustule into something more compatible with a photovoltaic system, enhances its abilities to function in a solar cell.

This thesis describes a four-step process: isolating and purifying diatom frustules, converting the material of the frustule into material that is more compatible with a photovoltaic system, assembling a functional solar cell, and testing it under a solar simulator. I will summarize in brief each of these processes here.

In the first step, diatoms were isolated from other organic material and purified by removing the living material from the exoskeleton (frustule). Samples were soaked in 2-propanol over night to kill all living material in the sample, including crustaceous organisms, algal plants, and other unidentified organisms. Algal leaves were then soaked in a warm bath containing 10%

hydrochloric acid to remove the mucus adhering the diatoms to algal leaves. These samples were then run through a sieve to remove large organic matter, and finally, the last of the organic residue was removed via an over-night bath of near-boiling 30% aqueous hydrogen peroxide. Cleaning was confirmed via a color change from green to white, and visually under the microscope.

Second, the diatom frustules were coated in TiO_2 to make them conductive. This was achieved by using peptide mediated deposition, a method previously established by Rorrer et al [1][2]. This deposition was confirmed using both a Time of Flight Secondary Ion Mass Spectrometer (TOF-SIMS) and a scanning electron microscope (SEM) equipped with EDX (Energy Dispersive X-Ray Analysis). The TOF-SIMS provides elemental, chemical state, and molecular information on the surfaces of solid materials. It does this by exciting a samples' surface with a finely focused ion beam which causes secondary ions and ionized clusters to be emitted from the samples surface. A time-of-flight analyzer is used to measure the mass of the emitted ions and clusters. From the mass and the full width at half-max of the SIMS peak, the identity of an element or molecular fragments can be determined. The average depth of analysis for a TOF-SIMS measurement is approximately 1 nm [38]. Under the TOF-SIMS we had an average uncorrected ion count Ti/Si ratio of 2.5 (range of .54—4.6) Ti/Si. The SEM provides detailed high-resolution images of the sample by using a focused electron beam along the sample's surface and detecting secondary or backscattered electron signals. The depth of the SEM's scan depends on the accelerating voltage and the material of the sample in question. An Energy Dispersive X-Ray Analyzer (EDX or EDA) is also used to provide elemental identification and quantitative compositional information [39]. Using EDAX on the SEM we got an average atomic count Ti/Si ratio of .14±0.05 Ti/Si.

For the third part of this experiment, we assembled prototypes of two solar cells: hybrid polymer nanoparticle, and dye sensitized (DSSC). While the hybrid polymer nanoparticle solar cells never reached a functional state, much work was done on establishing a functional prototype. This work can be found in the Appendix. For the DSSCs, fully functional cells were assembled using Fluorine-doped Tin Oxide (FTO) glass, TiO_2 with ruthenium absorbed onto the surface, an iodide electrolyte, and a pencil-graphite back electrode.

Finally, experiments were carried out under an in-lab solar simulator, using a Light Emitting Diode (LED) peaking at 550nm. Data was collected on the short circuit current (Isc), the open circuit voltage (Voc), the Fill Factor (FF), Efficiency, and Spectral Absorbance. More details about what each of these variables are will be discussed in the Solar Cell Results section 4.3.b.

Chapter 2: Theory

2.1 Solar Cells

Solar cells (SCs) are categorized into three main categories which are separated based on performance and cost effectiveness. First generation solar cells can be thought of as the silicon based SCs which currently dominate the market. They currently have the highest efficiencies and most expensive production costs. First generation solar cells function through the photoelectric effect: a photon enters the active layer of the SC and excites an electron-hole pair from the donor (traditionally n-type) material. The electron-hole pairs are separated at the p-n junction of the doped semiconducter. The electron migrates through the conduction bands of the n-type material while the hole moves to the acceptor material (p-type, usually a monocrystalline silicon wafer). This conduction is driven by the electric field created in the SC with the build up of electrons at one electrode. Electrons are thus conducted through the active layer of the SC to the electrode, generating an electric current. Second generation solar cells are usually categorized by any thin film solar cell based on CdTe or CulnGaSe [40]. They have lower efficiency, and lower production costs and a less extensive fabrication process. Both first and second generation solar cells have a theoretical limit of 30% efficiency due to their single p-n junction.

2.2 3rd Generation Solar Cells—DSSCs

Third generation SCs cover a wide range of experimental PV devices which do not use expensive silicon wafers, and are not limited to 30% efficiency. Two third generation SCs of interest in this thesis are Hybrid Polymer/Nanoparticle Solar Cells and Dye Sensitized Solar Cells. Dye-Sensitized Solar Cell (DSSC) are currently one of the most promising type of 3rd generation solar cell. They exibit several advantages over traditional silicon solar cells, such as: simple and inexpensive fabrication processes, and power generation under low light situations [3]. Because of the DSSC's ambient stability, and ease of preparation, they are an ideal model device platform for investigating the potential of diatoms to enhance light trapping in photovoltaic devices.

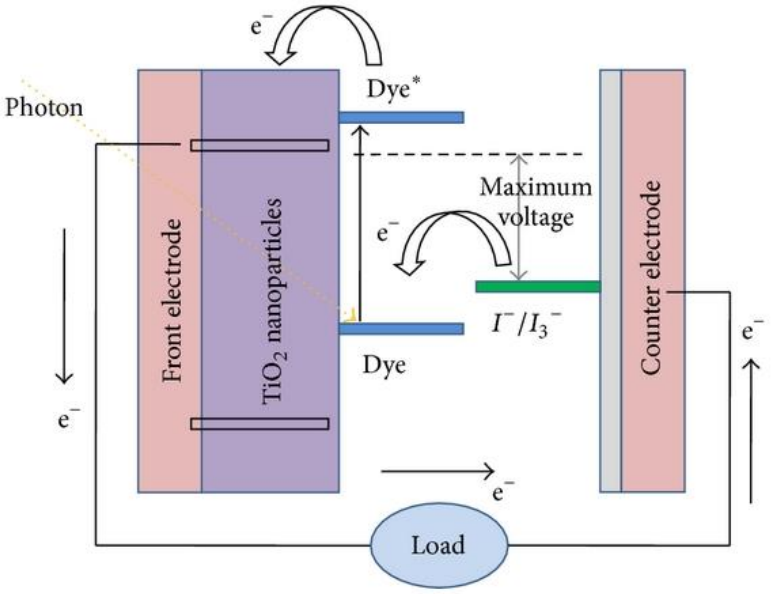

Figure 2: Materials, architecture, and bandgap alignment of a DSSC [12]

There are many available references which summarize the structure and function of a DSSC [10] [11]. In brief: to produce photocurrent in a DSSC, the photosensitizing dye, typically a metal-based ruthenium-polypyridine complex with absorption tuned to the visible spectrum but centered at 400-500 nm, absorbs a photon. Because it is bound to a layer of TiO_2 in its photoexcited state it can inject an electron into the conduction band of the semiconducting TiO_2 nanocrystal, creating an electron-hole pair. The electron is transported across the conduction band of the titania layer to a transparent conductive-glass front electrode and then performs work when passed through a load. The electrons then re-enters the cell by conversion of the electrolyte from I_3^- to $3I^-$ at the back electrode [4] and replenishes the dye. An example of the structure and band-gap diagram can be seen in figure 2, where the electron moves from the dye's conduction band into the conduction band of the TiO_2, and from there is transported through the circuit, back into the counter electrode which acts as a catalysis in the redox reaction that the electrolyte undergoes to replenish the depleted dye molecule. Note the fact that the dye molecules' valence band must lie above that of the TiO_2, and the electrolyte's conduction band must lie above that of the dye's in order to drive electron flow.

The processes undergone in a DSSC can be understood with the following four steps:

Excitation of the Dye Molecule by a photon

(1) $S+h\nu \rightarrow S^*$

Injection of an electron from the dye into the TiO_2

(2) $S^* \rightarrow S^+ + e^-$

Regeneration of the dye molecule by the iodide electrolyte

(3) $2S^+ + 3I^- \rightarrow 2S + I_3^-$

Regeneration of the iodide electrolyte at the counter electrolyte

(4) $I_3^- + 2e^- \rightarrow 3I^-$

Where S is a dye molecule, and S* is an excited dye molecule. [11].

There are also pathways where energy can be lost (back transfer pathways) which govern the efficiency of the cell [12]. These include:

Excited electrons in the dye falling back to ground state

(1) $S^* \rightarrow S$

Regeneration of the dye by the electron which had been injected into the TiO_2

(2) $S^+ + e^- \rightarrow S$

Recombination of electrons injected into the TiO_2 with I_3^-

(3)) $I_3^- + 2e^- \rightarrow 3I^-$

The thickness of the TiO_2 is another factor which governs device efficiency. The high internal surface area of the TiO_2 layer is one of the main factor governing the DSSC's performance. The higher the internal surface contact, the more places there are for the photon absorbing dye, the TiO_2 semiconducting charge carrier, and the electron-regenerating $3I^-/I_3^-$ electrolyte to contact, and thus promote the conversion of a photon to electric current. The thicker and more porous the TiO_2, the more area there is for these interface-contacts, and the more places there are for photon absorption. A thickness of at least 10 μm is usually required [11][17], however, this thickness reduces device efficiency since the TiO_2 nanoparticle layer must transfer charge to the conducting anode over a greater distance, and light attenuates as it moves through this layer. The diatom provides a novel source to potentially overcome these competing effects. The diatom's high surface area can increase the number of sites for internal surface contact, and, because of photonic crystal structure, it could serve to "trap" photons within the nanoparticle TiO_2 layer. Thus the TiO_2 layer could theoretically be expanded without affecting the device efficiency. [3][4][9]

Until now, the focus of improving DSSCs has been limited to optimizing either the structure of the titania layer, the photosensitizing dye, or the electrolyte [5]. The incorporation of diatom frustules into the photoanode has the potential to enhance DSSCs in a novel manner, specifically, by acting as an integrated reflector or photonic crystal. [6][4]. Jeffryes, et. al [4] outlines the different ways in which diatom frustules have been tuned in the past to maximize their ability to work in photovoltaic systems. After examining the following references which discuss different methods to alter the frustrule [4][5][7][8][9] and comparing that to the assembly methods and materials needed in 3rd generation solar cells, we decided to use Rorrer et. al.'s peptide-mediated deposition, because of its reported relative ease, safety of materials required, low cost, and reported reproducibility. We also chose to test a DSSC using materials which are low-cost. For this purpose, I assembled our DSSCs using pencil graphite as our back electrode. Ahmad, Shahzada, et. al's review article on different types of counter electrodes can be found here [13] and Cheng, Wei-Yun's review of carbon based counter electrodes specifically was used to find the optimal, and cheapest method for testing purposes [14]. The goal of this project is to

see whether diatoms can be used to increase the efficiency of our DSSCs, and whether or not there is a difference in the change of efficiency if the material of the diatom frustule has been altered. Because we are trying to measure the change in efficiency, not to maximize the efficiency in this experiment, low cost materials were deemed acceptable for testing purposes.

Chapter 3: Deposition of TiO_2 onto the Diatom Frustule

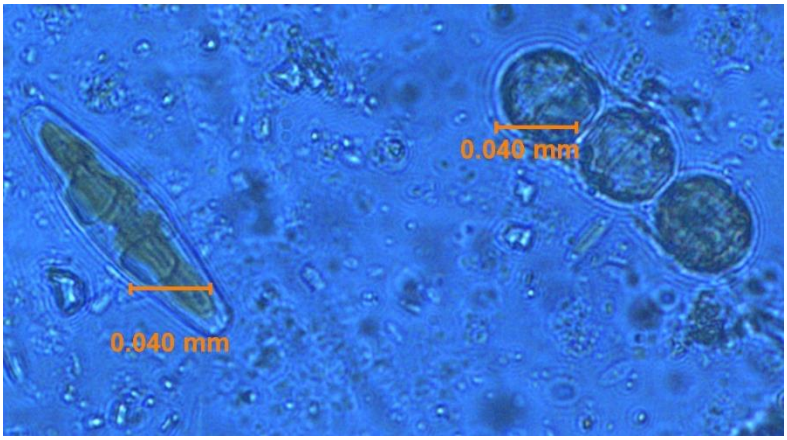

Figure 3: The two most common species of diatoms seen in the raw York samples. Left: pennate, Right: spherical (thalassiosira)

3.1 Isolation and Purification

The following procedure was used to isolate and purify our diatoms.

Algae was gathered from three different locations on the York River. The sample included three different species of algae brown, red, and green algae. Samples were then separated by species of algae, and were analyzed individually under the microscope to confirm a) that diatoms were present in each sample, and b) that the species present in each sample were similar. Two species were found to be most prevalent: a pennate species (football shaped), and a spherical species of the genus thalassiosira (thal). We were unable to identify the exact genus of the pennate species. Images of the most prevalent species before cleaning can be seen in figure 3, the pennate species is on the left, and a row of thalassiosira are on the right, linked together in a chain via a mucous membrane created during reproduction. After confirming that each sample had the same rough composition of diatoms, the samples were stored in 2-propanol overnight to kill all living organisms.

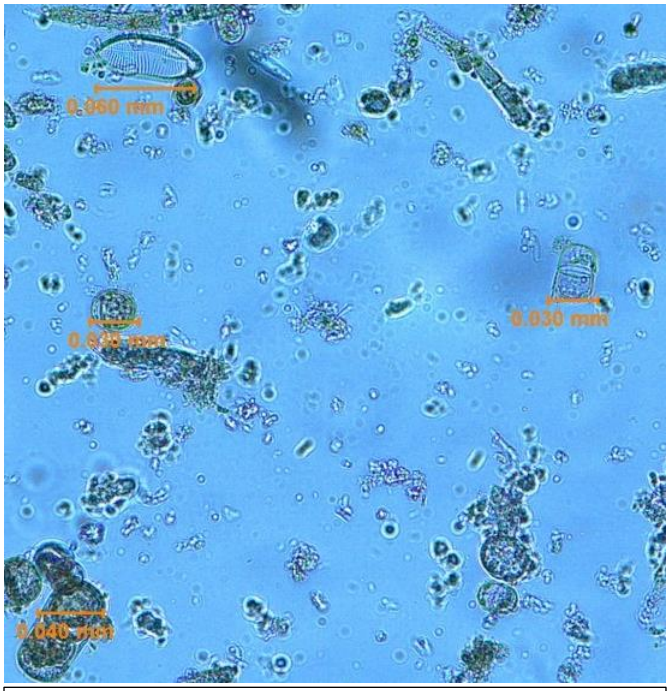

Figure 4: Diatom sample after isolation but before cleaning

Diatom Isolation:

Once the algae samples were examined, the diatoms then needed to be isolated. The proceedure for isolating the diatoms was as follows:

1. Drain samples to remove the alcohol and combined.
2. Cover with a thin layer of 10% HCl and submerge completely in deionized water (DI H_20).
3. Stir mixture periodically for 1.5hrs at a temperature just below boiling to dissolve the mucus adhering the diatoms to the algal leaves and one another.

4. Pour mixture through a sieve with a fine netting into a collection jar.
5. Wash tap water over the mixture until the water runs clear and dispose of material left in the netting.
6. Allow the solution to settle for one hour and then remove the supernant using a pipette to prevent the diatomaceous material from being disturbed.
7. Resuspend the remaining material in tap water. Repeat wash twice to remove the acid. Then repeated with Di H_20 twice, and allow the diatoms to settle overnight in Di H_20.

From here, a small sample was removed and viewed under the microscope to confirm the concentrated presence of diatoms. Results can be seen in figure 4, where it can be seen that diatomacious material was maintained, along with some organic material as well.

Ditaom Cleaning: The procedure to clean the diatoms was as follows:

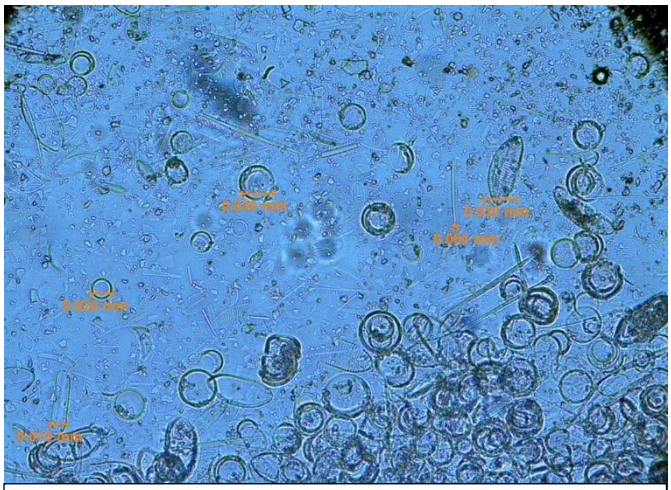

Figure 5: Diatom samples cleaned in H_2O_2, note the increased concentration of pure diatomaceous material

1. Wash diatoms again in Di H_20, this time via centrifugation, 3 times (200 rpm for 5 min).
2. Transfer 30g of wet cell mass to a 250 mL beaker and add 110 mL of 30% H_2O_2.
3. Place in a shaker at 78^{o}C and 125rpm for 24 hrs to remove organic matter from the biosilica frustrule. Cleaning should be confirmed by a visual color change in the cell mass from green to white.
4. Wash samples via centrifugation (600 g, for 15 min) in Di H_20 four times, Methanol 3 times, and then spin down once to help with drying.
5. Dry samples under flow with a vacuum over night.

Images of the cleaned cells can be seen in figure 5, note that only the frustrules of the diatoms remained after cleaning.

3.2 Peptide Mediated Deposition

The following procedure was used to coat our diatoms in TiO_2. An example of the proposed concept of this deposition as proposed by Rorrer et. al. can be seen in figure 6.

1. Wash an 80 mg aliquot of diatom biosilica isolated by the hydrogen peroxide treatment above four times with phosphate-buffered saline (PBS) in 0.1 M NaCl (PBS buffer, pH 7.9) by repeated centrifugation (200 g, 15 min) and resuspension.

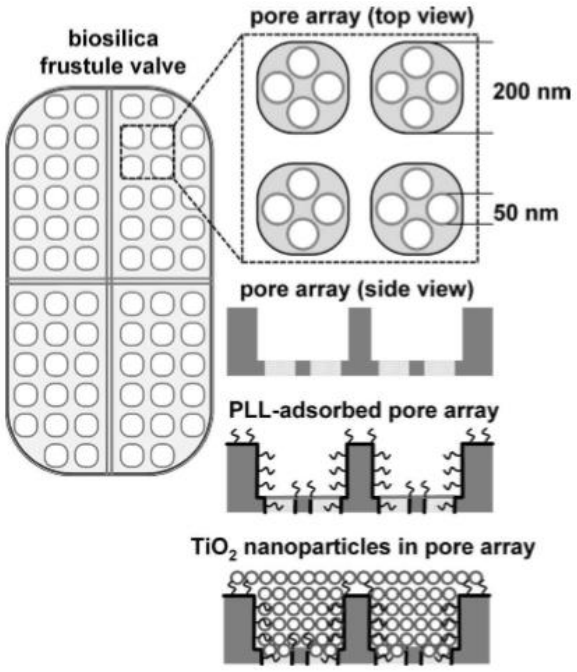

Figure 6: Concept of PLL-mediated deposition of TiO_2 onto diatom frustule biosilica as proposed by Rorrer et.al [1]

2. After the final washing, dilute the diatom biosilica suspension to 30 mL with PBS buffer in a 50 mL polypropylene centrifuge tube.
3. Add 10 mg of PLL (poly-L-lysine HBr from Fisher Scientific (Poly-L-Lysine Hydrobromide [MW 4,000-15,000], MP Biomedicals) to the diatom biosilica suspension and allow to adsorb onto the frustule biosilica surface under gentle mixing on multitube rotator plate at 30 rpm for 12 h at room temperature.
4. Wash the PLL-adsorbed diatom biosilica four times with PBS buffer as described above to remove unbound PLL from the solution.
5. To initiate the TiO_2 deposition, add 250 µL of 2.07 M titanium(IV)-bis(ammonium lactato) dihydroxide (Ti-BALDH) solution (50% w/v aqueous solution from Sigma-Aldrich 388165, mol wt. 294.12) to the PLL-adsorbed diatom biosilica (80 mg/30 mL PBS buffer) to provide an initial concentration of 17 mM Ti. Mixture is placed on a multitube rotator plate for 90 min under gentle, continuous mixing on a multitube rotator plate at 30 rpm at 22 °C to carry out TiO_2 deposition reaction.
6. Wash all samples four times with distilled water by repeated centrifugation (200 g, 15 min) and resuspension in PBS buffer to remove unreacted Ti-BALDH or unbound titanium precipitates. (Note: Original procedure called for nine washes; however, this was found to be too wasteful in terms of losing diatom cells. The purpose of the nine washes was to remove free titanium precipitates in the solution. This was done to ensure that they did not attract lysine during the second coating process. Four washes were sufficient for this purpose, as shown in our results section from the high amount of TiO_2 absorbed onto our diatoms)
7. Repeat steps 3-4 to absorb the PLL onto the diatom and then absorb the titania out of concentration in order to add a second layer of TiO_2 to the diatom biosilica.
8. Load the remaining sample into a crucible and anneal in air at 680 °C for 2.0 h within a small furnace.

3.3 Confirming Deposition

Samples were then analyzed using a Time of Flight Secondary Ion Mass Spectrometer (TOF-SIMS) and a scanning electron microscope (SEM) equipped with EDX. TOF-SIMS images were obtained over the range of 0-1000 daltons, and a total time of 2min. SEM images were obtained on a Hitachi S-4700 field emission scanning electron microscope (FESEM) equipped with EDX at an accelerating voltage of 25 keV, a distance ranging between x130-150K, and all EDX were taken for 100s.

Method for loading:

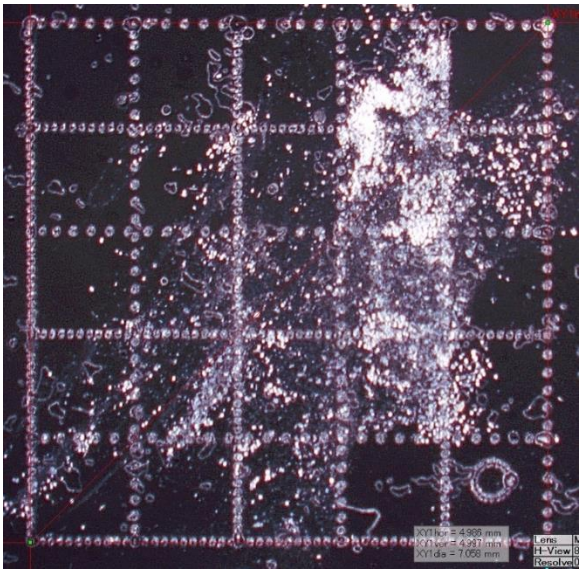

Figure 7: Example of the grid burned into the carbon tab via a laser cutter

We wished to examine the same diatoms in both the SEM and the TOF-SIMS. We also had a hard time locating diatom samples on the TOF-SIMS because of the low visibility on the apparatus. Because of these two factors, we developed a method for loading the diatoms that would allow us to locate the same diatom under both apparatuses. First, a 5x5 grid was burned into a carbon tab using a small laser cutter. Each box was 1mmx1mm. A circle was burned into the bottom corner for orientation purpose. Lines were of alternating width to help identify which side of the grid we were viewing. An example can be seen in figure 7. The white material seen in the figure are the diatoms. Sections where there was low diatom density were preferred to prevent charging in the SEM, and to ensure the proper diatom was being imaged in the TOF-SIMS.

Coated-diatoms were mounted onto a carbon tab by gently dipping a clean spatula into the dry, coated-diatom sample and tapping it above the carbon-mounted aluminum tab. Once loaded onto the carbon tab, several specific diatoms were found, from both species, using a microscope, and their location on the grid measured and recorded. This was repeated for a sample of uncoated diatoms as well. Measurements were taken on the elemental composition of both samples under the SEM and TOF-SIMS

3.4 Results on the TiO_2 deposition

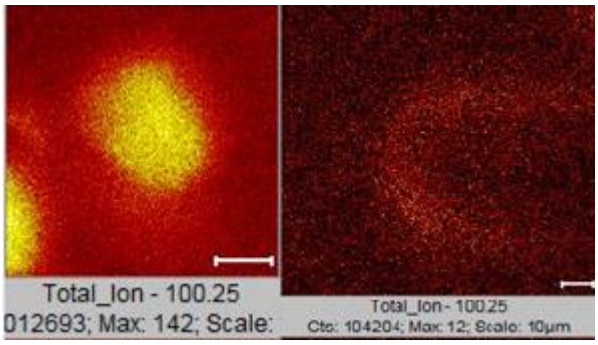

Figure 8: An example of diatoms as seen under the TOF-SIMS. Left: a coated thalassiosira, Right: an Uncoated thalassiosira

We used ion counts to compare the Ti:Si ratio on the coated diatoms to uncoated diatoms using the TOF-SIMS. This was done because we believe the TiO_2 to be deposited primarily on the surface of the diatom. The TOF-SIMS is designed for elemental surface analysis. Two samples of coated thalassiosira and two samples of coated penates were compared to one uncoated sample of each species. Fewer uncoated samples were examined because they were difficult to locate on the TOF-SIMS since they did not have any TiO_2 to make them visible (an example of what the coated diatoms look like under the TOF-SIMS versus the uncoated can be seen in figure 8. On the left, the titanium on the coated frustrule causes it to glow brightly, making it easy to find even if the camera is not centered over it. On the right, the uncoated frustrule does not glow brightly, which makes it difficult to locate unless the camera is centered directly over top of it). A bar graph comparing the Ti:Si ratio for each sample can be seen in figure 9.

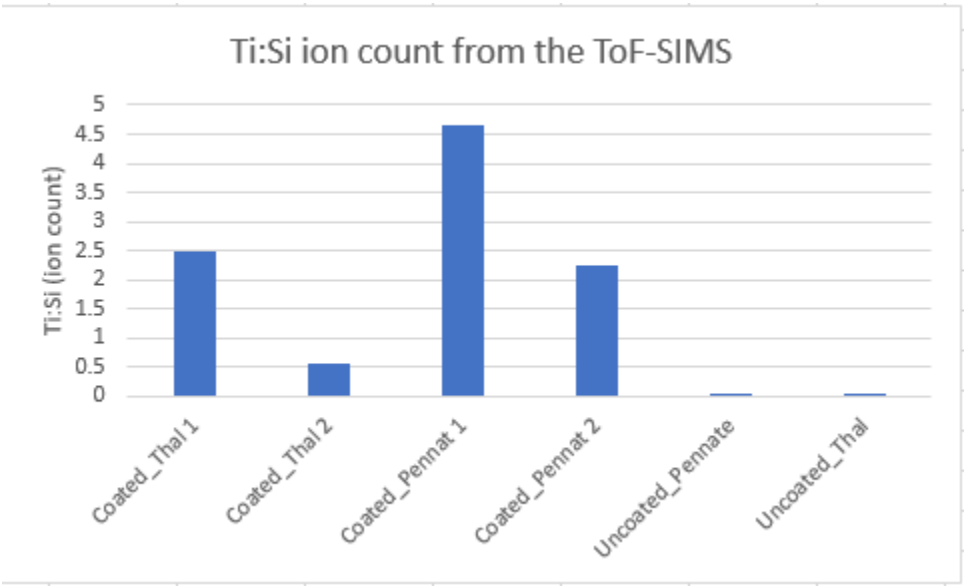

Figure 9: Ti:Si ratios for coated and uncoated samples taken from the TOF-SIMS

Statistical analysis to compare the average Ti:Si ratio for the coated vs uncoated samples, was not done as the sample size was too small. From observation it can be seen that there is a significant increase in the ratio of Ti:Si in the coated samples than the uncoated.

We had some questions about whether or not the coating process would be equally successful for both species of diatoms. While we are unable to perform statistical analysis on the TOF-SIMS data, given the low sample size, the variation from cell to

cell is large enough that there is no obvious trend that resembles a difference in the deposition between species at this time.

The mean Ti:Si atomic count ratio for the coated diatoms found under the TOF-SIMS was then 2.5 Ti:Si, over a range of .54—4.6 Ti:Si.

A more common method of elemental analysis is generally done using an SEM. To compare our results to that of Rorrer et. al, and also to gain some more understanding of where the TiO_2 was deposited (the high accelerating voltage we were using to prevent charging meant that many of the primary electrons were traveling deep into our samples, the exact depth being dependent on the sample density and elemental composition.) EDAX readings were taken to compare the ratio of Ti:Si on the coated diatoms using the SEM between three coated diatoms of both the pennate and thalassiosira species and one of each species of the uncoated samples. A scanning rate of 25KeV was found to be needed to prevent charging issues, which was more than Rorrer et. al. used, and thus it is difficult to directly compare our results to theirs. The SEM results, however, still give valuable information on the nature of the TiO_2 deposition. For

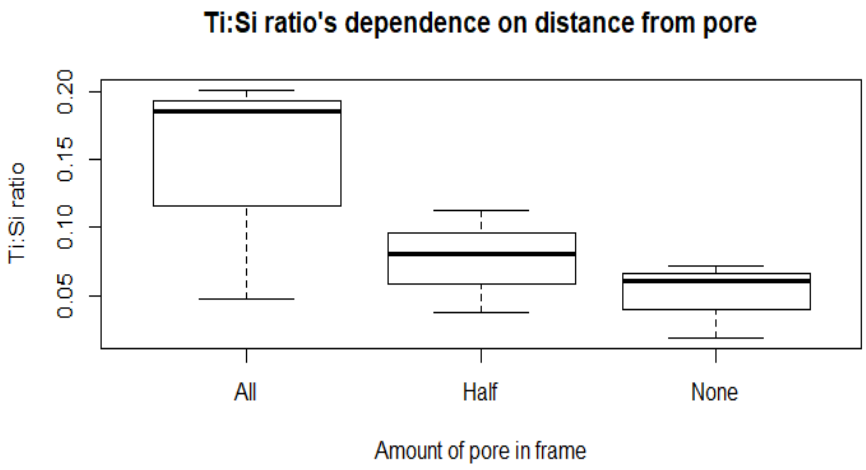

Figure 10: measure of the Ti:Si ratio as dependent on distance from pore for the Penates. Note that 'All' means centered directly over pore, while 'None' means centered directly over ridge.

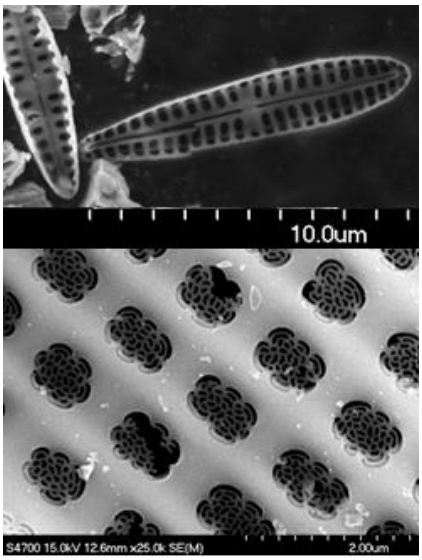

Figure 11: Top: An overview of a pennate frustule. Bottom: Close-up on the pores of said pennate frustule. There is an interesting lattice structure over each pore in the periodic structure.

example, it was suggested by Rorrer that the deposition occurred largely in the pores of the diatoms [1]. To determine if this was true, we wanted to see if the concentration of Ti:Si was dependent on the amount of pore which was in the scanning field. For an example of this pore structure, see figure 11. In this figure, the top image is an over-view of an entire pennate frustrule, where one large defining ridge runs down the center line of the cell, and smaller ridges run perpendicular to this center ridge to create rows of pore structures. In the bottom image, we

are close up on one of those pore structures, where the hierarchical pore structure can be seen, and there is a lattice of biosilica material across the inside of every pore. We tested the hypothesis that more TiO_2 was being deposited in the pore by taking EDAX scans of three pennate frustules while moving the camera off of the edge of the pore. One image was taken with the camera centered directly over the pore (all), one with only half of the pore in frame (half) and one directly over top of a ridge (none). Results can be seen in figure 10. The data does not provide sufficient evidence to suggest that the TiO_2 coating is more successful in the pore of the pennate frustules. Note that this type of analysis was not necessary for the thalassiosira as they do not have defined ridges. For consistency, the data used for analysis on the penates was centered over a pore such that 100% of the camera was occupied by the pore.

Edax was also taken over an uncoated sample of both species. Much less data was taken for the uncoated species due to charging issues on the SEM since they were non-conductive. A bar graph comparing the Ti:Si ratio for the coated penates, coated thalassiosira, and the uncoated

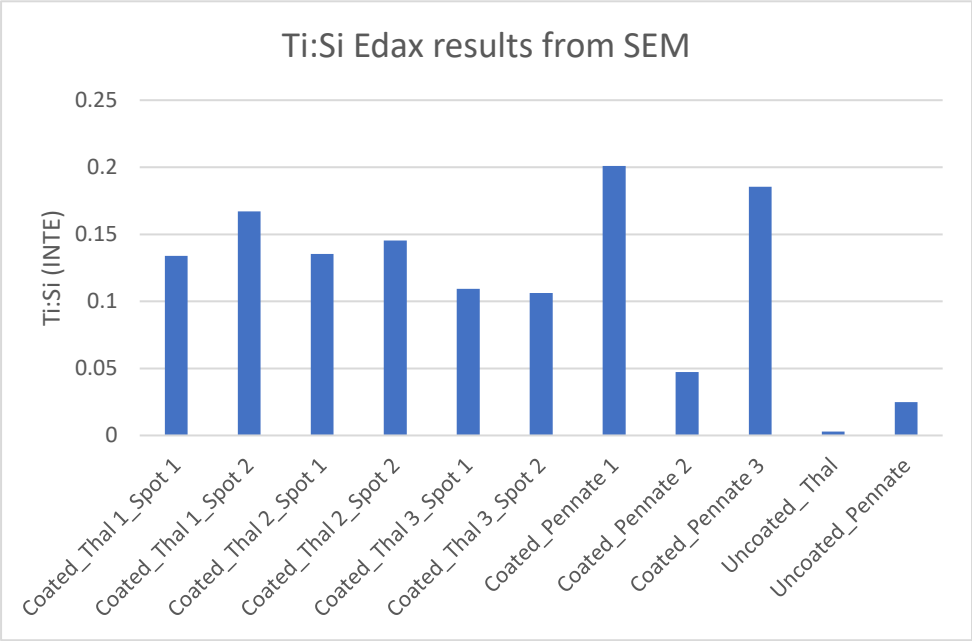

Figure 12: Ti:Si INTE Edax results comparing the coated to uncoated samples

species can be seen in figure 12, and example spectrums for one of the coated thalassiosira and the uncoated pennate can be seen in figures 13 and 14 respectively.

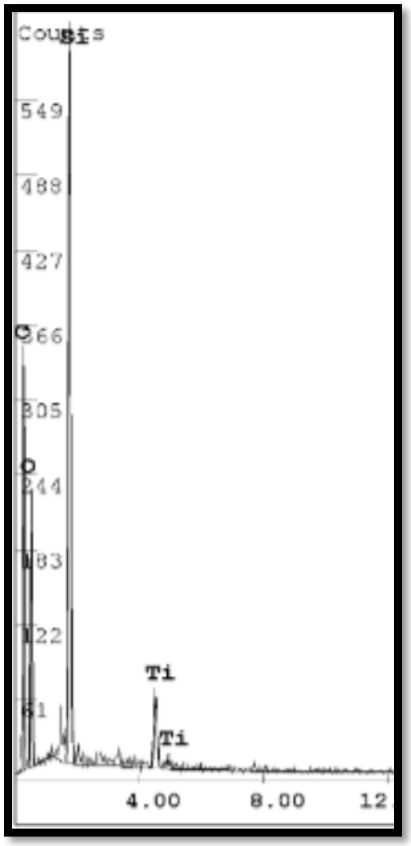

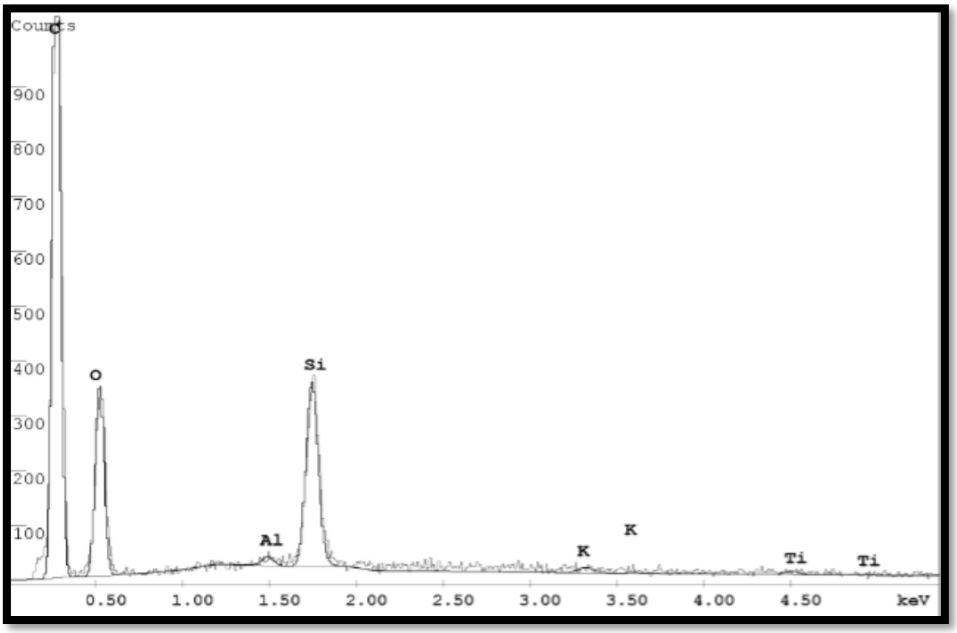

Figure 13: Spectrum for Coated Thal frustule one.

Figure 14: Spectrum for uncoated pennate frustule one. Note that the aluminum spike is likely due to the aluminum stub the samples were mounted on and the potassium is likely left over from the deposition process

The signal seen in the uncoated pennate frustule is believed to be an error caused by the spectral matching of the EDAX to trace amounts of material. To confirm this, the Ti counts compared to background were examined for the uncoated pennate, uncoated thal, the pennate sample with the smallest Ti:Si ratio, and the thal frustrule whose spectrum can be seen in figure

13. Results can be seen in table 1. Note that the uncoated samples have a Ti count much lower than the background, while the coated samples yield a Ti count higher than the background.

Table 1: Comparison of Ti count to Background Noise

Cell	**Ti (INTE)**	**Ti background (INTE)**
Uncoated Thal	.51	1.36
Uncoated Penn	.79	1.36
Coated Penn 2 (lowest)	.97	.26
Coated Thal	7.91	.45

Again, note that a statistical analysis to compare the coated and uncoated samples was not useful, given that only two samples of the uncoated frustules were available. Due to this no statistical comparisons were made. Looking at our samples there is a large variation between the coated and uncoated samples—especially given the uncoated pennate samples Ti count compared to background. Because of this, we conclude that there is a higher Ti:Si ratio for the coated samples than for the uncoated samples. Again, statistical comparisons were not done to test whether there is a difference in the efficiency of the deposition process for different species. At this time, our data does not show any obvious trends that would indicate a difference in the deposition between diatom species.

The mean Ti:Si atomic ratio for the coated diatoms found under the SEM was .14±0.05 Ti:Si.

The method we used to deposit TiO_2 on the surface of our diatoms was adapted from a method developed by Rorrer et. al. at Ohio university. Rorrer's results as reported in his paper on diatom integration into a DSSC [2] had a Ti:Si ratio of 0.77 ± 0.05 g TiO_2 / g SiO2 as determined by ICP analysis (Inductively Coupled Plasma mass spectrometry). Note that this is a weight to weight comparison, not a surface comparison. The literature and our results indicated that the TiO_2 is deposited on the surface only of the diatom, as indicated by the significantly larger Ti:Si ratio we achieved under the TOF-SIMS as opposed to the SEM. ICP analysis would not be preferred to get a true understanding of the TiO_2 layer in this case. In addition, such a large weight ratio would only make since if there were extremely large stacks of TiO_2 in the pore of the frustrule. This was not what our data indicated was true. This which is why we chose for our method of analysis to make a true surface comparison of the ratio of atomic counts.

Chapter 4: Assembling and Testing the Solar Cells

4.1 Assembling the Solar Cells

Over the course of this thesis project, two different types of solar cells were made: Hybrid Polymer/Nanoparticle solar cells and Dye-Sensitized solar cells. The original plan for this thesis was to use Hybrid Polymer Nanoparticle solar cells; however, I was never able to make a functioning prototype. Eventually, we decided to leave the hybrid cell for later research, since we estimated that the work needed to make a functioning prototype would take more time than was left to complete this thesis. The appendix lists the procedures and results from this portion of the project.

The Dye-Sensitized solar cells were made with the intention to test whether or not diatoms increased the efficiency of a solar cell, and whether or not there was evidence that coating the frustrule in TiO_2 would boost this increase. Because of this, we used less traditional, low-cost materials, such as a graphite counter-electrode instead of the usual platinum. Some attempts were made to create a carbon-black counter electrode (.035 g of graphite and .168 g of carbon black in 3 mL of isopropanol and 3 mL of Polyethylene glycol, screed across the surface of the cell to form a continuous layer, and annealed at 450 C for 30 min); however, we were unable to stop this solution from separating during the annealing process. Because of this, we chose to use pencil graphite to make our counter electrode. The other materials and procedure for assembly of a prototype cell with no diatoms in the TiO_2 layer were as follows:

Preparing the Iodide Electrolyte:

1. Dissolve .127 g of Iodine (I2) in 10 mL of poly-ethylene glycol, then add .83 g of Potassium Iodide (KI) and stir.
2. Store electrolyte in a dark, amber vial at room temperature and stir thoroughly before use.

Preparing the TiO_2 precursor:

1. Add 3 g of TiO_2 nanoparticle precursor (Titanium(IV) oxide, anatase, nanopowder, <25 nm particle size, 99.7% trace metals basis, Sigma Aldrich) to 5 mL of Polyethylene glycol and stir with a mortar and pestle until smooth and lump-free (approx. 5min).
2. Add 2 mL of 10% HCl to act as an anticoagulant.
3. Allow mixture to sit for 15 min before immediate use, and then stored in a sealed amber vial at room temperature. Stir mixture thoroughly before each subsequent use.

Applying the TiO_2 electrode:

1. Mask 3mm of the conductive side of FTO glass (~10 ohms/square, 25*25 mm,>79% transmittance, Tech Instro) with scotch tape.
2. Deposit 3-5 drops of the TiO_2 solution in a row on one side of the slide, and use a clean glass rod to draw the solution across the slide to create a thin, uniform layer.
3. Allow slides to dry for 5 min before removing the tape.
4. Anneal the slides by placing them on a hot-plate and slowly increasing the temperature to 350 ^oC. A quick color change should be observed from white to dark brown, and annealing is confirmed after the slide has changed back to white. The entire process lasts anywhere from 30 min-1 hr.

5. Thickness of the layer was measured using a filmetrics surface profilometer to be approximately 80 microns. This can be seen in figure 16. No pinholes were seen in any layer.

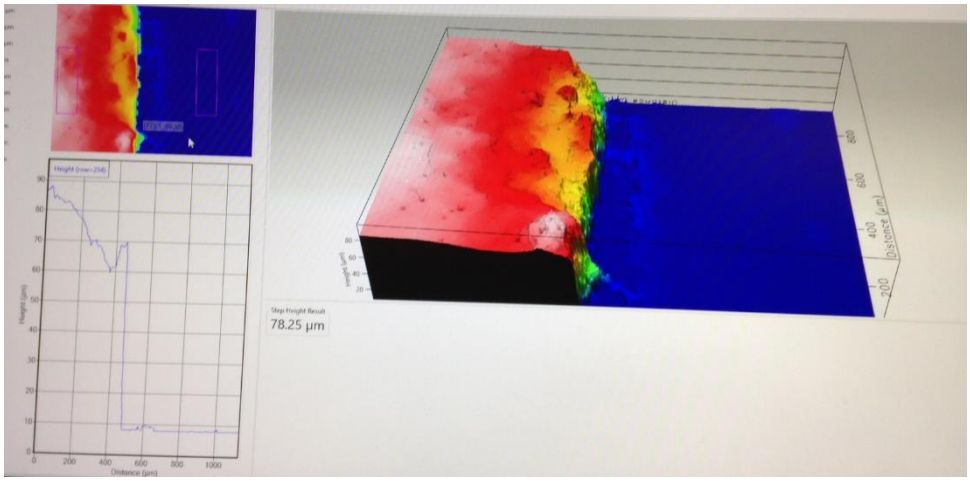

Figure 16: Thickness of the TiO_2 layer as measured on a surface profilometer. Thickness was found to be the difference between the flat glass and the area where the TiO2 layer begins to level, which can be seen in the overview in the top left corner. Averaging over three measurements gave us approximately ~80 micron thickness

Activation with Dye:

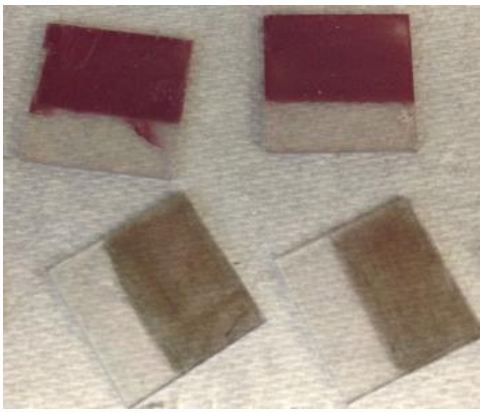

1. Dissolve the dye in isopropanol to a concentration of .3 mg/mL and sonicate for 5min.
2. Place the TiO_2 electrode face up in the dye solution for 2hrs at room temperature.
3. After removing the slide from the solution, rinse the excess dye off with isopropanol, and then allowed them to sit and dry in the air.

Figure 17: Dye-Sensitized TiO_2 layers and Graphite Electrodes. Ruthenium on top, graphite layers on the bottom

Assembling the Back Electrode:

The back electrode was deposited onto 2/3 of the conductive side of a piece of Fluorine doped Tin Oxide (FTO) glass by direct pressure on the graphite point of a #2 pencil by first tracing the pencil horizontally, then vertically, then making small circles across the coated area. 1/3 of the side was left unetched for measurements.

Figure 18: Fully assembled cell. The cell can be seen being held upright with

Assembling the full cell:

1. Carefully place the TiO_2 and graphite electrodes against one another, ensuring that at no point the uncoated FTO glass on either side contacts, and hold together with clamps.
2. Deposit 1-3 drops of the iodide electrolyte solution on the edge of the two slides, and draw into the slides using capillary action by alternately opening and closing the clamps.
3. Once the electrolyte covers all parts of the inner cell, wipe the two electrodes clean.

Images of our dye-absorbed TiO_2 layers, graphite layers, and a fully assembled cell can be seen in figures 17 and 18 respectively.

Several methods were used to incorporate diatoms into the active layer of the cell, and all were tested to see which gave the best performing cell. A description of each of these procedures, and the resulting cell efficiencies can be found in the results section 4.3.b.

4.2 Testing

First our solar cells were determined to be functional by measuring them for diode-like behavior using a GAMRY Reference 600 potentiostat/galvanostat/zra.

IV curves were taken using a tafel test. In a tafel test voltage is varied across the electrodes and the resulting current is measured. On a single electrode the Tafel equation can be stated as $\eta = Aln(\frac{i}{i_o})$ where η is the overpotential, A is the tafel slope, i is the current density and i_o is the "exchange current density." We observed these plots for rectification in one direction, that is, current flowing more easily for either positive or negative voltages. This confirmed that our cell had unidirectional flow.

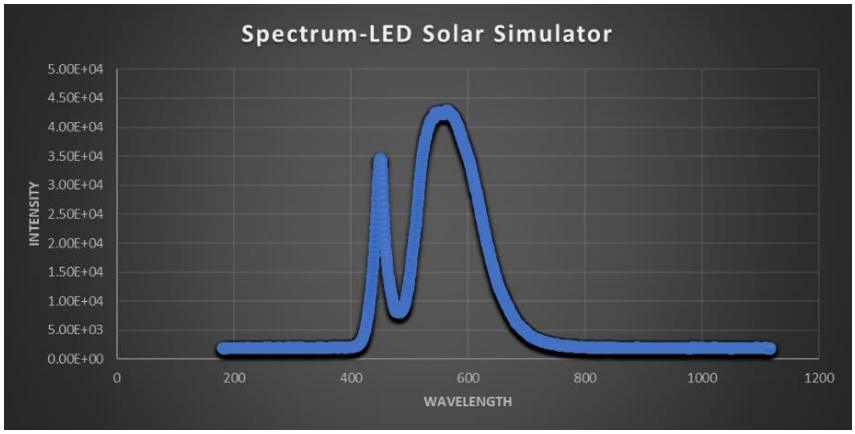

Figure 19: Spectral Output from our LED. Main peak is at 550nm

Testing on the solar cells was done with an LED light source peaking at 550nm (110V, 4W, GU10 LED Bulbs - 6000K Daylight Spotlight - 330 Lumen). A spectrum of our LED can be seen in figure 19, which was measured using a Steller Net, SpectraWiz spectrometer, Raman-HR-TEC-405. I made several setups of our in-house solar simulator, including one which used 11 LEDs in a hexagonal pattern, as recommended in [16]. This set-up was preferred for higher illuminance; however, the set-up we found to be the best for spectral uniformity used only one LED, since, as is discussed in our results section below, a higher illuminance was not preferred for our testing. Spatial uniformity was found by measuring the Isc using an iris aperture to block the light from all but a small circle of light (r=56mm). The Isc was taken with the spot of light shining in the top left corner, the top right, the center, bottom right, and bottom left. The measurement was repeated at different lengths of separation between the LED and the solar cell until a coefficient of variation less than 10% was reached. This was found to be any distance farther than 42cm away.

The goal of our experiment was to see how the addition of our diatoms affected the overall efficiency of our cell, so an attempt was not made to estimate the spectral mismatch of our simulator to the standard 1.5 AG spectrum (the solar spectrum as measured from 1.5 atmosphere thickness, corresponds to a solar zenith angle of z=48.2°), especially as a 1.5 AG simulator was not available to us; however, data was taken on a standard control cell under our simulator and sunlight and the mismatch could be calculated if it was deemed necessary in the future.

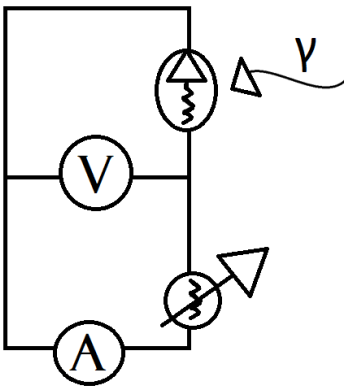

An equivalent circuit diagram of our setup can be seen in figure 20. In summary: the voltage was measured across our solar cell in series with a voltmeter, while the current was measured in parallel using a picoameter. A variable resistor was used in series with the picoameter to create our IV curves. Data was also taken of the background light for each test and subtracted from the final I-V curve. Neutral density filters were used to verify the linear dependence of our current on the illuminance as is discussed in the results section 4.3.9.

Figure 20: Measurements were taken with the above configuration. The DSSC is measured as a diode in series with a resistor, the voltage is measured in series, the current is measured in parallel and a variable resistor was used to create our IV curves.

A typical IV curve can be seen in figure 21 where the power produced by the cell in Watts can be easily calculated along the I-V sweep by the equation P=IV. At the ISC and VOC points, the power will be zero and the maximum value for power will occur between the two. The voltage and current at this maximum power point are denoted as VMP and IMP respectively [37].

Note that there are three variables which contribute to the power output of a solar cell: illuminance, temperature, and solar spectrum. Current should increase linearly with increases in current. Changes in solar spectrum will effect current. Finally, increases in temperature will cause Voc to decrease, thereby decreasing max power [37]. An ideal photocell would have a perfectly square IV curve.

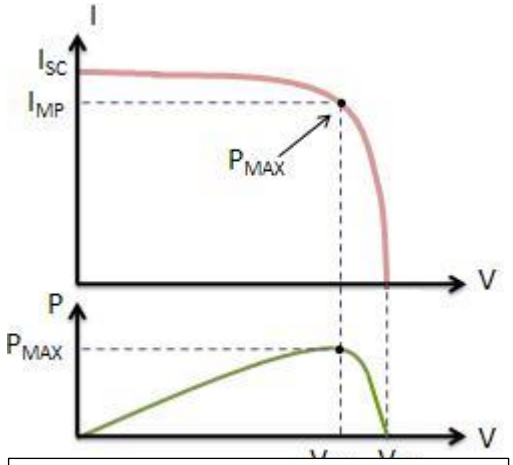

Figure 21: Maximum power for an IV sweep can be seen as the location where current begins to change a lot with small changes in voltage.

4.3 Results From testing the Solar Cells

4.3.a Saturation Current

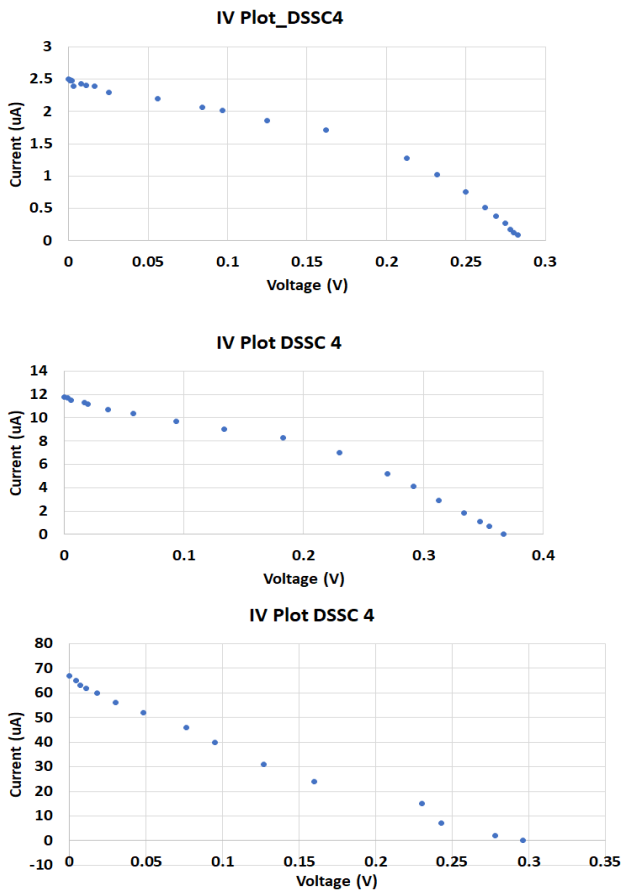

Figure 22: An example of the non-linearity of current to light intensity. Light intensity is highest for the bottom picture, and lowest for the top. Note that the higher intensity causes the 'squareness' of the plot to decrease.

While testing prototype cells which did not contain diatoms, it was noticed that the Fill Factor ($P_{max}\frac{I_{sc}}{V_{oc}}$)—a measurement of the 'squareness' of our data) was dropping rapidly as the illumination on the cell was increased. An example of this can be seen in the IV plots in figure 22, where, as the intensity rises, the 'squareness' of the plot begins to drop.

To find a place where the solar cell's current responded linearly to light intensity, plots were taken at various light intensities by using Neutral Density Filters (NDF). Specifically, the level of NDF would be increased until the Isc was thought to be behaving linearly. At that point an IV curve was plotted, then a .3 NDF was inserted and another IV curve plotted to see if the current dropped by approximately ½. NDF's attenuate light across the electromagnetic spectrum by 10^{NDF}. The IV plot that was taken with the .3 NDF was rescaled to compare to the plot without the .3 NDF. This can be seen in figure 23. As one can see, with the higher light intensity (NDF .6) when a .3 NDF was added, and the plot re-scaled, it did not perfectly match with the original IV line. However, at lower intensities (1.0 NDF) when a .3 NDF was added, and the plot rescaled, the IV plots did match up. Because of this, all future measurements were taken in a range where the IV plot was linearly dependent on light intensity. This meant that higher levels of input were not preferred (as discussed in our experimental set-up section).

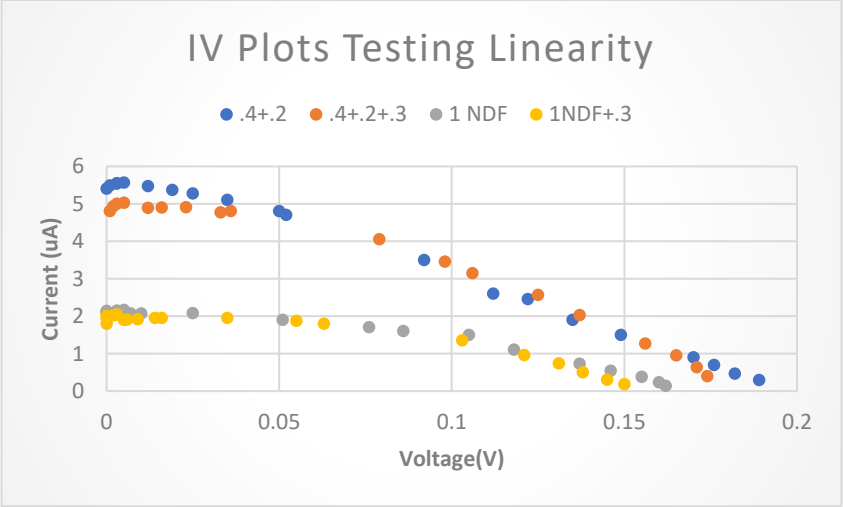

Figure 23: Plots to test linearity of the IV plots as dependent on Pin. IV plots were taken at two different light intensities using NDF's. Then a .3 NDF was added, which should have reduced the current by 1/2. These plots were rescaled to see if the entirely of the IV plot was behaving linearly.

This saturation problem would prevent our cells from ever operating at their full efficiency under solar illumination. In addition, given that it was hypothesized that the addition of diatoms would increase the number of photons in the DSSC's active layer, we hypothesized that the addition of diatoms may increase the saturation problem. A saturation problem of this kind is not discussed in the literature, and so we hypothesized a series of mechanisms that might be causing the saturation.

Our first hypothesis was that the problem may have been occurring due to poor dye absorption onto the TiO_2 layer. To test this, I deposited a layer of TiO_2 onto an FTO slide, and then placed the slide vertically in a dye solution for 2hrs, such that only the lower half had been exposed to the dye. I then shone a green laser light through the sample and recorded the spectrum and intensity using the SpectraWiz photometer. The green laser had three peaks: one at 532nm, one at 805nm, and one at 1,064nm. We measured the relative intensity for both halves of the sample (one with dye, and one without), at three different spots, and took the average for peak intensity. We then divided these by the peak intensity for the green light by itself to get the percent transmittance. Results can be shown in table 2.

Table 2: % transmittance of green laser through a sample that had a TiO_2 layer where half was exposed to Ruthenium. Calculated as peak intensity of sample/peak intensity of green light alone

%Transmittance-Ruthenium Dye		
Peaks Wavelength(nm)	**TiO2 No dye**	**TiO2+dye**
532	4.083%	0.557%
805	9.918%	1.828%
1064.5	5.64%	2.953%

As is shown, for the peak occurring at 532, the one associated with the visible green, there was a transmittance decrease of .136%, giving us an absorption of approximately $e^{-6.6}$. Given that Ruthenium has an absorption length of approximately $10^4 M^{-1}cm^{-1}$ [36] we can calculate the molarity of our absorption as follows:

$$Absorption\ Length = \frac{1}{L}$$

Where L is length. Therefore

$$10^4 M^{-1} cm^{-1} = \frac{1}{L}$$

For us, the absorption is $e^{-6.6}$ and absorption is found as $e^{-X/L}$ where X is thickness of the TiO_2 and L is the absorption length. Setting these equal to each other we get X=6.6L and given that we know X~80 microns, we can calculate L to be .0012cm. Plugging this into the above equation we get

$$10^4 M^{-1} cm^{-1} = \frac{1}{.0012\ cm}$$

This gives us a molarity of approximately .0833 moles/L. Given a starting concentration of $\frac{.3mg}{mL} * \frac{1mol}{1188.55g} = 2.5 * 10^{-4} mol/L$, this is a very high absorption, which makes it unlikely that our transmittance problem is being caused by a lack of dye molecules.

We can also look at the time to regeneration of our dye, by using this result and the known photon energy to calculate the number of photons a molecule would need to absorb per second. Given the area of our laser to be 6.22mm^2 and the thickness of our layer to be .008cm, we calculate the number of molecules in our sample to be

$$.0833 \frac{mol}{liter} * (.0622 * .008) cm^3 = 4.146 * 10^{-5} mol$$

$$6.022 * 10^{23} \frac{molecules}{mol} * 4.146 * 10^{-5}\ mol = 2.497 * 10^{19} molecules$$

Given that the energy of the green light at 530nm is 6.3mW, we can calculate the number of photons hitting our sample per second to be

$$6.3mW * 530nm * \frac{1}{ch} = 1.67 * 10^{16} photons/second$$

Where c is the speed of light in a vacuum and h is Plancks constant.

This means one molecule of dye would need to absorb a new photon every 1,495 seconds. Given this relatively large time between absorption, a lack of dye is likely not the source of our saturation problem.

The mechanics of a saturation current are often largely governed by recombination at one of the three interfaces (dye to TiO_2, the TiO_2/dye to electrolyte, or electrolyte at the back electrode) [12]. Recombination mechanics are normally governed by the temperature of the cell, as increases in temperature will shift the bandgap alignment between the TiO_2 and the dye [12]; however, this is likely not what is causing our saturation problem for us, as we are using an LED at a large distance away from our cell, so increases in illumination have minimal changes in temperature. Additional research into TiO_2 thickness revealed that as the TiO_2 layer's thickness is increased, the chance of recombination with the dye is also increased [10][17]. We hypothesized that this was what might be causing our saturation. To get a better understanding of this saturation current we developed the following procedure to analyze the saturation constant in our cells: at the resistance corresponding to the maximum power for each cell, we varied the light intensity over a series of P_{in}, starting with 0, one point at the linear regime of the cell, and several points far past the end of the linear range until a clear saturation is seen. We tested this procedure for cells without diatoms and with coated, and uncoated diatoms (see results section 4.3.b for discussion on diatom integration, and 4. 3.c for the assembly of the cells seen in figure 24). Results can be seen in figure 24. As hypothesized, the inclusion of diatoms only increased the saturation constant.

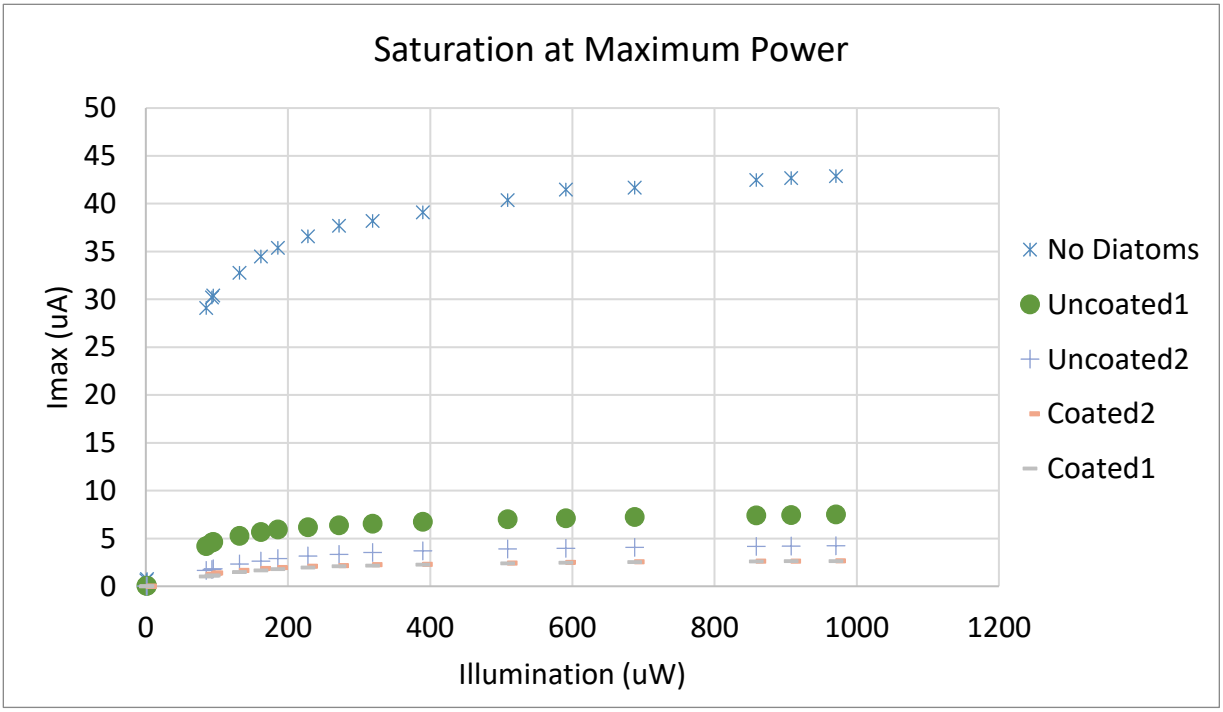

Figure 24: The current at max power plotted for varying levels of light intensity, starting just at the edge of the linear regime and plotting well into the range of saturation. This measurement taken for several cells including those which contained diatom frustules that were both coated in TiO_2 and not coated in TiO_2.

This result alone may have continued to suggest that the mechanism governing this saturation was due to recombination; however, we also repeated this measurement with zero resistance, and recorded the I_{sc} as a function of light intensity, results seen in figure 25, and here we found that the current varied linearly with light intensity.

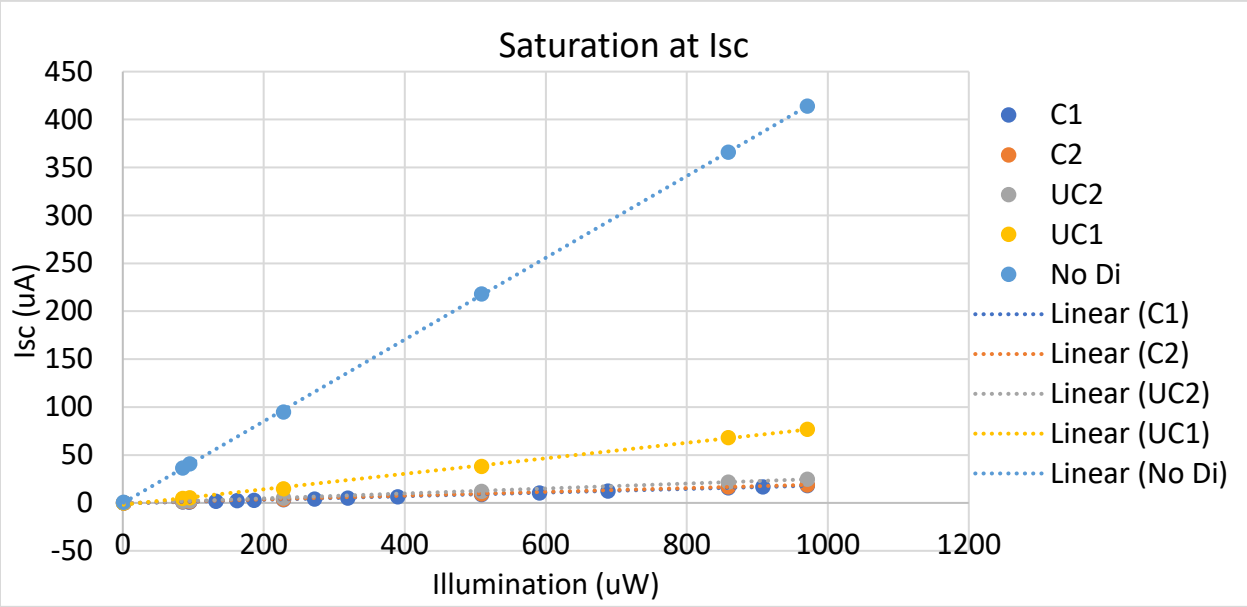

Figure 25: The short circuit current plotted for varying levels of light intensity, starting just at the edge of the linear regime and plotting well into the range of saturation. This measurement taken for several cells including those which contained diatom frustules that were both coated in TiO_2 and not coated in TiO_2.

This indicated that the problem was not due to recombination, as recombination issues would cause the saturation to be seen along the entire IV curve. This indicates that our IV plots are behaving as though the series resistance (seen in figure 26) is current dependent.

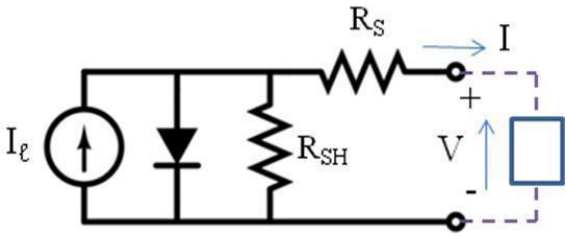

Figure 26: Simplified Equivalent circuit model for a photovoltaic cell [37]. Rs=Series resistance, and Rsh=Shunt resistance

At low light levels our solar cells behave as one would expect, however, at high light levels the current at maximum power begins to drop while the I_{sc} remains linear. This suggests that the series resistance has increased. We are not losing electrons due to recombination, as shown with our high Isc levels, which means that we are likely losing energy where the electrons are flowing out through the TiO_2 or back into the iodide. Normally resistances tend to not be dependent on current, although they can change with temperature changes. We show a marked increase in series resistance. The exact origin of this resistance increase is not clear, and future experiments should examine the conacts and look for any sort of preferential heating on one surface or the other at high light illumination. Another experiement that future research may

want to conduct is to run a current through the cell to check that the resistance is dependent on current. Further experimentation will be required to better understand this saturation behavior.

4.3.b Incorporating Frustules into DSSCs

Despite the saturation problem, the goal of the experiment was to test the effectiveness of diatoms in enhancing the efficiency of our DSSCs, so cells were assembled using both coated and uncoated frustules. A universal protocol for incorporating diatoms into a DSSC is not established, and papers which have used diatoms in DSSCs thus far [2] [3], use dissimilar procedures. For this purpose, we tested 4 methods of integration using the uncoated diatoms: First, uncoated diatoms were mixed to a concentration of .055g frustule material/300 µL of PEG, then the following methods were used for assembling the full cell:

(A) 2 layers of a diatom suspension that was made with a 50:1 weight ratio diatoms to TiO_2 solution

(B) One layer of TiO_2 with a layer of 50:1 weight ratio diatoms to TiO_2 on top

(C) One layer of 50:1 (weight ratio) diatoms to TiO_2 with a layer of TiO_2 on top

(D) A single layer of diatom solution mixed with a weight ratio of 1:1.5 diatoms to TiO_2

Cells B and C were made to replicate the work done by Rorrer et. al [2] and Huang et. al [3] respectively, cells A and D were made based on our own hypothesis for performance. Each of these were tested under the LED lamp in ranges where the Isc was linearly dependent on light intensity. The results are summarized in table 3. For every cell tested, the following variables were taken/calculated:

- Cell Area: $Length \times width\ of\ the\ active\ layer\ of\ cell$
- Isc: Short Circuit current
- Voc: Open circuit voltage
- FF: $\frac{I_{sc}}{V_{OC}} P_{max}$ (a measurement of the 'squareness' of our data)
- Illuminance: Light shining on the cell. $Power\ reading\ from\ the\ photometer / area\ of\ the\ photometer\ aperture$
- Pin: Power into the cell. $Illuminance\ \times Cell\ area$
- Pmax: point at which IV is maximum. Found by varying R.
- Eff: $Pmax/Pin$
- Eff%: $Eff \times 100$
- NDF is the neutral density filter used to ensure that we were in a regime where current behaved linearly with increases in illumination.

For more information on any of these characteristics, an excellent guide to solar cell properties and measurements was written by National Instruments [37].

As one can see in table 3, by a large factor it was found that the higher TiO_2 Concentration (Cell D) yielded the highest efficiency. We believe this to be the case because the uncoated diatom-only layers were likely insulating electron flow, and the increased TiO_2 concentration helped provide more areas for electron flow. Thus, this was the method decided upon for the final cells which were assembled for both coated and uncoated diatoms.

Table 3: Testing the best method for the incorporation of diatoms into our solar cells. Note that cell A was nonfunctional

Cell	Assembly Method	NDF	Isc	Voc	FF	Illuminance (uW/mm^2)	Pin (uA)	Eff	Eff%
A	2 layers of uncoated diatoms mixed with a little TiO2 (50:1)	N/A	N/A	N/A	N/A	N/A	N/A	N/A	N/A
B	Layer of TiO2, then a layer of diatoms on top	1	8.7	0.402	0.533596	6.410256	1201.016	0.001554	0.155385
C	Layer of diatoms, then a layer of TiO2 on top	0.6	0.54	0.202	0.342868	2.820513	285.2949	0.000131	0.013109
D	1 Layer of uncoated diatoms mixed in a 1:1.5 ratio with TiO2	0.9	5.9	0.405	0.58	0.794	82.5	0.01679	1.67

4.3.c Final Solar Cells

For the purpose of comparing whether or not there is evidence that diatoms increase the efficiency of our DSSC, and to test whether or not conversion of the frustule material aids in efficiency enhancement, six solar cells were made: two without diatoms, two with uncoated diatoms, and two with coated diatoms. The completed cells were then tested under the LED at ranges in which the current behaved linearly with illumination, the same variables from section 4.3.b were also found here. Cells were not all completed on the same day, which is important to note as that may affect the consistency in the assembly process (discussed below).

Saturation analysis on these cells can be seen in section 4.3.a in figure 24, and shows that as hypothesized, the addition of diatoms does seem to increase the saturation problem. Final results may be affected by the saturation problem, discussed earlier, and as such, these results should be retested after a solution to the saturation problem has been found.

Results can be seen in table 4.

Table 4: Final results comparing solar cells without diatoms, with uncoated diatoms, and with coated diatoms

Cell	NDF	Cell Area (mm^2)	Isc	Voc	FF	Illuminance (uW/mm^2)	Pin (uW)	Pmax	Eff	Eff %
No Diatoms1	1	296.6	37.5	0.43	0.570	1.543	457.8	9.22	0.0201	2.01
No Diatoms2	1	303.8	29.2	0.43	0.583	1.543	469.0	7.32	0.0156	1.56
Uncoated1	0.9	103.8	5.9	0.405	0.580	0.794	82.5	1.38	0.0167	1.67
Uncoated2	0.9	108.4	2.9	0.327	0.491	0.794	55.0	0.33	0.0056	0.56
Coated 1	0.9	69.2	2	0.327	0.500	0.794	59.2	0.39	0.0067	0.67
Coated 2	0.9	74.5	2.4	0.335	0.491	0.794	86.2	0.47	0.0054	0.54

As can be seen, there is no evidence that adding diatoms to the solar cell has increased the efficiency, nor that conversion of the frustule material has benefits for PV activity. Absorption and transmission data was taken for each of the above samples (calculated the same was as in section 4.3.a) and can be seen in figure 27 and table 5 respectively.

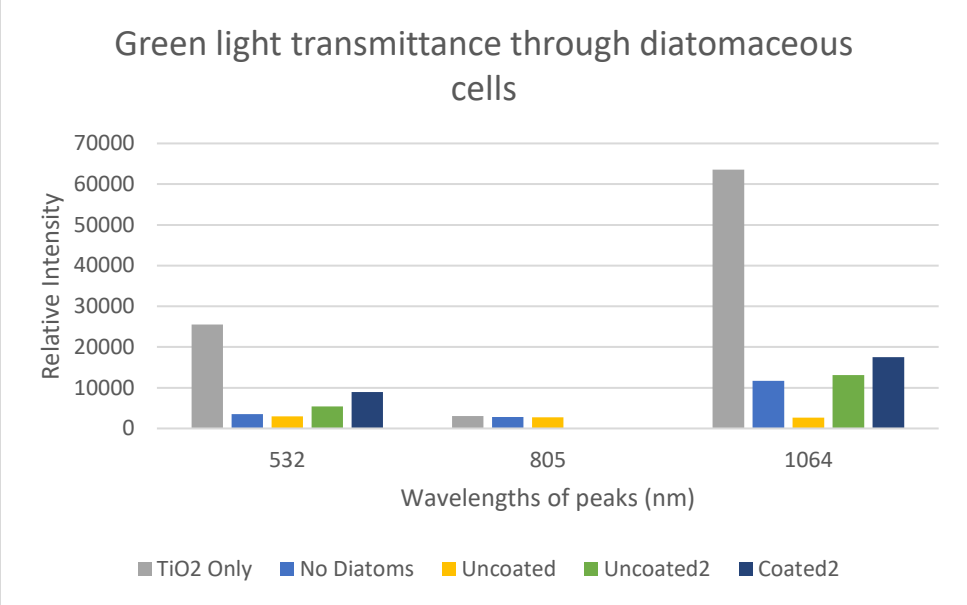

Figure 27: Absorption of cells without dye, with dye and no diatoms, with uncoated diatoms, and with coated diatoms. Increases in the amount of absorption between the No diatom cells and other diatom cells indicate inconsistencies in our assembly process

Table 5: Percent transmittance of our solar cells. Calculated as intensity of respective sample/intensity of green light alone

%Transmittance					
Peaks Wavelength	**TiO_2 No dye**	**TiO_2+dye**	**Uncoated 1**	**Uncoated 2**	**Coated 2**
532	4.083	0.557	0.470	0.863	1.427
805	9.918	1.828	0.417	2.044	2.732
1064.5	5.64	2.953	2.373	13.98	10.268

There appears to be some correlation to the amount of dye absorbed and the efficiency of the solar cell. While in some cases it seems that the addition of the diatoms increased dye absorption, this is not consistent across all samples. In fact in some cases, the amount of transmission increased for some of the diatomaceous cells. This transmission measurement is also affected by the thickness of the TiO_2 layer, since the TiO_2 was deposited by hand, in many cases the thickness varied and affected the starting amount of light allowed to pass through the sample. The variations in the absorption and transmission of these samples, indicates there are inconsistencies in our assembly process.

This raises a larger issue with our assembly process. Inconsistencies due to the number of steps involved in this assembly process likely affected our results. Our assembly process made it difficult to exactly reproduce results. To test consistency, measurements were taken of four prototype cells that were assembled using a rhodamine dye (Results seen in table 6), the mean efficiency between them was calculated to be 0.01408%, with a standard deviation of 0.007331, giving us a coefficient of variation of 52%. Coefficients of variation below 10% are usually desirable in any sample set. This inconsistency is a large problem that affects the credibility of our results, and is likely to be improved by developing a method to better deposit a consistent thickness of the TiO_2 layer.

Table 6: Measuring the variability of performance due to our assembly process. Four cells made over the course of two different days. Note: These cells were made with a Rhodamine dye

Cell	NDF	Isc	Voc	FF	Illuminance (uW/mm^2)	Pin (uW)	Eff	Eff %
1	0.3	1.591	0.263	0.393	7.69	1894.1	8.7E-05	0.00870
2	0.3	1.095	0.255	0.455	7.69	2348.4	5.42E-05	0.00542
3	.9	1.07	0.176	0.356	1.44	359.4791	0.000187	0.0186
4	.9	1.75	0.19	0.370	1.44	520.7773	0.000237	0.0236

There are two common methods to develop a procedure for consistent TiO2 thickness. The first is Spin-Coating, which is discussed in the appendix in the section on layer characterization (also see Daniyan [33], Suciu [34], and Ossila's spin-coating guide [35]). The second would be to gain access to a commercially produced Doctor-Blader where thickness levels can be set, rather than doctorblading by hand. Note that for thicknesses which are small enough, one may have trouble getting an accurate measurement of the thickness using the filmetrics surface profilometer due to transparency issues. Another method for using the PHENOM for thickness measurements can be found in the appendix in the section on layer characterization.

Conclusion

The goal of this experiment was to see whether or not it was possible to enhance the abilities of a DSSC using wild-type diatoms, and to see whether or not converting the material of the frustule would enhance the ability to increase DSSC efficiency.

A successful procedure was developed to clean and deposit TiO_2 onto the surface of the frustules, using near-boiling baths of hydrogen peroxide and a peptide-mediated deposition method. This procedure was developed and refined so that it can be accomplished by any following researcher in under three weeks, from algae collection to testing on the TOF-SIMS. In addition, TiO_2 deposition was found to be largely successful, giving us an average Ti:Si atomic count ratio of 2.5±1.7 Ti/Si under the TOF-SIMS. Statistical analysis determined that the coating process is equal for both species of diatoms, and further testing using an SEM suggests that the location of the TiO_2 nanoparticles is along the surface of the frustule, due to the much larger ratio of Ti:Si from the TOF-SIMS than on the SEM.

DSSCs were then assembled: Two with no diatoms, two with uncoated diatoms, and two with coated diatoms. The cells without diatoms were found to have an efficiency of 1.78% ± .23%, the uncoated diatoms cells were found to have an efficiency of 1.11% ± .57%, and the coated diatoms cells were found to have an efficiency of .6311% ± .04%. These results do not show any indication that the diatoms have increased the efficiency of the solar cells at this time, nor is there any evidence that altering the frustrule material is advantageous for solar cell efficiency.

Several problems were also discovered during the process of assembling and testing the DSSC's. The first is a large saturation current at high light intensities which we hypothesize to be caused by energy loss at one of the contacts. The other is inconsistencies in the assembly process, largely caused by the fact that the TiO_2 layer is being doctorbladed by hand. Further testing to confirm the cause of the saturation current, and developing a procedure to increase consistency across samples, are two things that should be improved upon for further testing. Possible methods to solve both of these problems are suggested in the results section of this paper.

Citations

1: Jeffryes, Clayton, et al. “Peptide-Mediated Deposition of Nanostructured TiO_2 into the Periodic Structure of Diatom Biosilica.” *Journal of Materials Research*, vol. 23, no. 12, Nov. 2008, pp. 3255–3262., doi:10.1557/jmr.2008.0402.

2: Rorrer, Gregory, et al. “Peptide-Mediated Deposition of Nanostructured TiO_2 into the Periodic Structure of Diatom Biosilica and Its Integration into the Fabrication of a Dye-Sensitized Solar Cell Device.” *Materials Research Society Symposium Proceedings*, 2009, doi:10.1557/proc-1189-mm02-05.

3: Huang, Der-Ray, et al. “Enhancing the Efficiency of Dye-Sensitized Solar Cells by Adding Diatom Frustules into TiO_2 Working Electrodes.” *Applied Surface Science*, vol. 347, 2015, pp. 64–72., doi:10.1016/j.apsusc.2015.04.064

4: Jeffryes, Clayton, et al. “The Potential of Diatom Nanobiotechnology for Applications in Solar Cells, Batteries, and Electroluminescent Devices.” *Energy & Environmental Science*, vol. 4, no. 10, 2011, p. 3930., doi:10.1039/c0ee00306a.

5: Chandrasekaran, Soundarrajan, et al. “Silicon Diatom Frustules as Nanostructured Photoelectrodes.” *Chemical Communications*, vol. 50, no. 72, 2014, p. 10441., doi:10.1039/c4cc04470c.

6: Chen, Xiangfan, et al. “Understanding the Nanophotonic Light-Trapping Structure of Diatom Frustule for Enhanced Solar Energy Conversion: a Theoretical and Experimental Study.” *Bioinspired, Biointegrated, Bioengineered Photonic Devices II*, Mar. 2014, doi:10.1117/12.2038529.

7: Unocic, Raymond R., et al. “Anatase Assemblies from Algae: Coupling Biological Self-Assembly of 3-D Nanoparticle Structures with Synthetic Reaction Chemistry.” *Chemical Communications*, no. 7, 2004, p. 796., doi:10.1039/b400599f.

8: Zhou, Han, et al. “Biotemplated Materials for Sustainable Energy and Environment: Current Status and Challenges.” *ChemSusChem*, vol. 4, no. 10, Sept. 2011, pp. 1344–1387., doi:10.1002/cssc.201100048.

9. Su, Bao-Lian, et al. “Hierarchically Structured Porous Materials for Energy Conversion and Storage.” *Hierarchically Structured Porous Materials*, 2011, pp. 577–600., doi:10.1002/9783527639588.ch19

10: Shalini, S., et al. “Status and Outlook of Sensitizers/Dyes Used in Dye Sensitized Solar Cells (DSSC): a Review.” *International Journal of Energy Research*, vol. 40, no. 10, 2016, pp. 1303–1320., doi:10.1002/er.3538.

11: Ahmad, Muhammad Shakeel, et al. “Advancements in the Development of TiO 2 Photoanodes and Its Fabrication Methods for Dye Sensitized Solar Cell (DSSC) Applications. A Review.” *Renewable and Sustainable Energy Reviews*, vol. 77, 2017, pp. 89–108., doi:10.1016/j.rser.2017.03.129.

12: Tripathi, Brijesh, et al. “Effect of Varying Illumination and Temperature on Steady-State and Dynamic Parameters of Dye-Sensitized Solar Cell Using AC Impedance Modeling.” *International Journal of Photoenergy*, vol. 2013, 2013, pp. 1–10., doi:10.1155/2013/646407.

13: Ahmad, Shahzada, et al. “Metal Free Sensitizer and Catalyst for Dye Sensitized Solar Cells.” *Energy & Environmental Science*, vol. 6, no. 12, 2013, p. 3439., doi:10.1039/c3ee41888j.

14: Cheng, Wei-Yun, et al. “Graphene Aerogels as a Highly Efficient Counter Electrode Material for Dye-Sensitized Solar Cells.” *Carbon*, vol. 54, 2013, pp. 291–299., doi:10.1016/j.carbon.2012.11.041.

15: Saxena, Vibha, et al. “Metal-Free Organic Dye for Dye Sensitized Solar Cells.” 2012, doi:10.1063/1.4710177.

16: González, Manuel I. “An LED Solar Simulator for Student Labs.” *Physics Education*, vol. 52, no. 3, 2017, p. 035002., doi:10.1088/1361-6552/aa5f86.

17. Zhang, Shufang, et al. “Highly Efficient Dye-Sensitized Solar Cells: Progress and Future Challenges.” *Energy & Environmental Science*, vol. 6, no. 5, 2013, p. 1443., doi:10.1039/c3ee24453a.

18: Kosyachenko, Leonid A. *Solar Cells: New Aspects and Solutions*. InTech, 2011.

19: Zhou, Yunfei, et al. “Organic-Inorganic Hybrid Solar Cells: State of the Art, Challenges and Perspectives.” *Solar Cells - New Aspects and Solutions*, Feb. 2011, doi:10.5772/19732.

20: Saunders, Brian R., and Michael L. Turner. “Nanoparticle–Polymer Photovoltaic Cells.” *Advances in Colloid and Interface Science*, vol. 138, no. 1, 2008, pp. 1–23., doi:10.1016/j.cis.2007.09.001.

21: Saunders, Brian R. “Hybrid Polymer/Nanoparticle Solar Cells: Preparation, Principles and Challenges.” *Journal of Colloid and Interface Science*, vol. 369, no. 1, 2012, pp. 1–15., doi:10.1016/j.jcis.2011.12.016.

22: Liu, Ruchuan. “Hybrid Organic/Inorganic Nanocomposites for Photovoltaic Cells.” *Materials*, vol. 7, no. 4, Feb. 2014, pp. 2747–2771., doi:10.3390/ma7042747.

23: Zeng, Tsung-Wei, et al. “A Large Interconnecting Network within Hybrid MEH-PPV/TiO2 Nanorod Photovoltaic Devices.” *Nanotechnology*, vol. 17, no. 21, 2006, pp. 5387–5392., doi:10.1088/0957-4484/17/21/017.

24: Bouclé, Johann, et al. “Hybrid Bulk Heterojunction Solar Cells Based on Blends of TiO2 Nanorods and P3HT.” *Comptes Rendus Physique*, vol. 9, no. 1, 2008, pp. 110–118., doi:10.1016/j.crhy.2007.10.005.

25: Zeng, Tsung-Wei, et al. “Hybrid Poly (3-Hexylthiophene)/Titanium Dioxide Nanorods Material for Solar Cell Applications.” *Solar Energy Materials and Solar Cells*, vol. 93, no. 6-7, 2009, pp. 952–957., doi:10.1016/j.solmat.2008.11.023.

26: Her, Hyun-Jung, et al. “Hybrid Photovoltaic Cell with Well-Ordered Nanoporous Titania–P3HT by Nanoimprinting Lithography.” *Journal of Physics and Chemistry of Solids*, vol. 69, no. 5-6, 2008, pp. 1301–1304., doi:10.1016/j.jpcs.2007.10.121.

27: Reeja-Jayan, B., and A. Manthiram. “Influence of Polymer–Metal Interface on the Photovoltaic Properties and Long-Term Stability of Nc-TiO2-P3HT Hybrid Solar Cells.” *Solar Energy Materials and Solar Cells*, vol. 94, no. 5, 2010, pp. 907–914., doi:10.1016/j.solmat.2010.01.021.

28: Kwong, C.y., et al. “Influence of Solvent on Film Morphology and Device Performance of Poly(3-Hexylthiophene):TiO2 Nanocomposite Solar Cells.” *Chemical Physics Letters*, vol. 384, no. 4-6, 2004, pp. 372–375., doi:10.1016/j.cplett.2003.12.045.

29: Park, Young Ran, et al. “Investigations of the Polymer Alignment, the Nonradiative Resonant Energy Transfer, and the Photovoltaic Response of Poly(3-Hexylthiophene)/TiO2 Hybrid Solar Cells.” *Journal of Applied Physics*, vol. 108, no. 4, 2010, p. 044508., doi:10.1063/1.3459889.

30: Wisnet, Andreas, et al. “Nanoscale Investigation on Large Crystallites in TiO2 Nanotube Arrays and Implications for High-Quality Hybrid Photodiodes.” *Journal of Materials Science*, vol. 47, no. 17, 2012, pp. 6459–6466., doi:10.1007/s10853-012-6580-2.

31: Kwong, C Y, et al. “Poly(3-Hexylthiophene):TiO2 Nanocomposites for Solar Cell Applications.” *Nanotechnology*, vol. 15, no. 9, Feb. 2004, pp. 1156–1161., doi:10.1088/0957-4484/15/9/008.

32: Muktha, B., et al. “Synthesis and Photocatalytic Activity of Poly(3-Hexylthiophene)/TiO2 Composites.” *Journal of Solid State Chemistry*, vol. 180, no. 10, 2007, pp. 2986–2989., doi:10.1016/j.jssc.2007.07.017.

33: Daniyan, Ayodele Abeeb, et al. “Preparation of Nano-TiO2 Thin Film Using Spin Coating Method .” *Journal of Minerals and Materials Characterization and Engineering*, vol. 01, no. 04, 2013, pp. 138–144., doi:10.4236/jmmce.2013.14024.

34: SUCIU, Ramona-Crina, et al. “TiO2 THIN FILMS PREPARED BY SPIN COATING TECHNIQUE .” *National Institute for Research and Development of Isotopic and Molecular Technologies, Department: Physics of Multifunctional Nanostructured Systems*, No 63-105 , 5 Nov. 2010, pp. 607–612. *Research Gate*, http://web.icf.ro/rrch/ .

35: “Spin Coating: A Guide to Theory and Techniques.” *Ossila*, www.ossila.com/pages/spin-coating.

36: Chaignon, Frédérique, et al. “Distance-Independent Photoinduced Energy Transfer over 1.1 to 2.3 Nm in Ruthenium Trisbipyridine–Fullerene Assemblies.” *New Journal of Chemistry*, vol. 29, no. 10, 2005, p. 1272., doi:10.1039/b506837a.

37: “Part II – Photovoltaic Cell I-V Characterization Theory and LabVIEW Analysis Code.” *Part II – Photovoltaic Cell I-V Characterization Theory and LabVIEW Analysis Code - National Instruments*, www.ni.com/white-paper/7230/en/.

38: “TOF-SIMS.” *TOF-SIMS Surface Analysis Technique | Physical Electronics (PHI)*, www.phi.com/surface-analysis-techniques/tof-sims.html.

39: “Scanning Electron Microscopy, Energy Dispersive X-Ray Analysis (SEM EDX EDA).” *Lucideon*, www.lucideon.com/testing-characterization/techniques/sem-edx.

40. Khan, Md Imran, "A Study on the Optimization of Dye-Sensitized Solar Cells" *Graduate Theses and Dissertations-University of South Florida Scholar Commons.* (2013). http://scholarcommons.usf.edu/etd/4519

Acknowledgements

I would like to thank the following people:

- Dr. William Cooke
- Dr. Dennis Manos
- Dr. Kristin Wustholtz
- Dr. Lukas Schmidt-Mende
- Jacob Gunnarson
- Amy Wilkerson
- Harry Eller
- Dr. Abigail Reft
- William Schubert
- Olga Trofimova
- Dr. Jordon Walk
- Dr. Kurt Williamson
- Dr. Rob Granger
- Dr. Jill Granger

Appendix

Theory

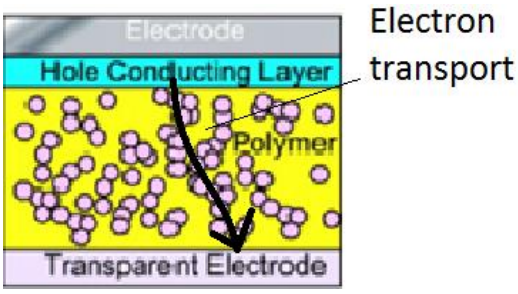

Figure 28: Example of the ideal morphology in a Hybrid Nanoparticle/Polymer SC. [22]

Third generation SCs cover a wide range of experimental PV devices which do not use expensive silicon wafers. For example, Hybrid Polymer/Nanoparticle SCs do not use separated p/n layers, but instead mix nanoparticles of acceptor material inside of the layer of donor, polymer material. The idea is that when the polymer generates an electron, if the nanoparticles are interspersed throughout it, this minimizes losses due to reabsorption [18], as seen in figure 28. The electron will not have as far to travel, and thus the active layer, the part of the SC containing the n and p material, can be expanded. This will allow for more incoming photons to be absorbed [18] [19]. Hybrid SCs have the potential to be one of the most cost-effective SCs on the market; however, they have been unsuccessful at reaching efficiencies that allow them to be economically competitive so far. This is largely due to assembly problems with the active layer; because of the nanoparticles' size they tend to clump together as the active layer is assembled. To reach maximum efficiency, the nanoparticles must be evenly dispersed throughout the polymer and form a continuous network for electron transport. Currently, the only way to achieve this particular structure is to use stabilizing ligands during the preparation of the active layer. Unfortunately these ligands are insulating and provide a barrier to charge transport [20][21] [22]. Upon comparison of the structure of the diatom frustule and the ideal dispersion pattern of the nanoparticles, I hypothesized that nanoparticles formed either inside of the pores of the diatom or along the diatom's surface could provide this hierarchical and constant structure without the need for insulating ligands. In addition, the diatom's unique optical properties could trap photons in the active layer, giving the SC a higher optical absorption than silicon cells. This would allow for increased efficiencies while still using simplistic, low temperature production methods. Finally, one of the most exciting prospectives of the diatomaceous Hybrid SC is that both the material of the nanoparticles, the silica frustrule and

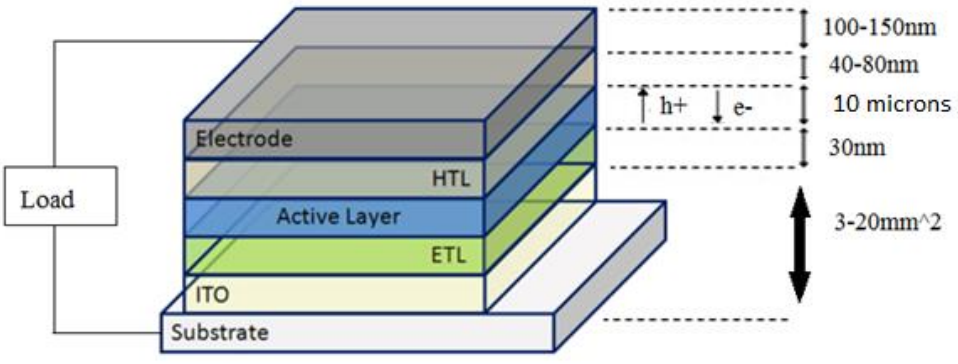

Figure 29: Hybrid polymer/nanoparticle layers and thicknesses

the polymer all have the potential to act as donors. This means that this style of SC has the potential for broad band absorption, and could function in low light conditions by absorbing photons well into the UV spectrum[5].

My literature review revealed a list of previous research that has successfully managed to absorb nanoparticles onto the frustrule of the diatom(see above section 2.2). I cross-refrenced this research with a list of common material-pairs used in the assembly of Hybrid SC's and decided that it would be best to assemble a SC using TiO_2 packed frustrules as the nanoparticles, mixed within P3HT polymer [23][24][25][26][27][28][29][30][31][32]. These are both relatively inexpensive materials that are non-toxic and easy to handle and store. In addition, there is an established protocol for easily absorbing TiO_2 onto the surface of the frustrule that has been shown to be photo-voltaicly compatiable (See Peptide Mediated Deposition in Chapter 3 above) that is relatively simple and could be verified using equipment to which we had access. P3HT is well documented, one of the easiest polymers to use, has band-gaps that align well with TiO_2,

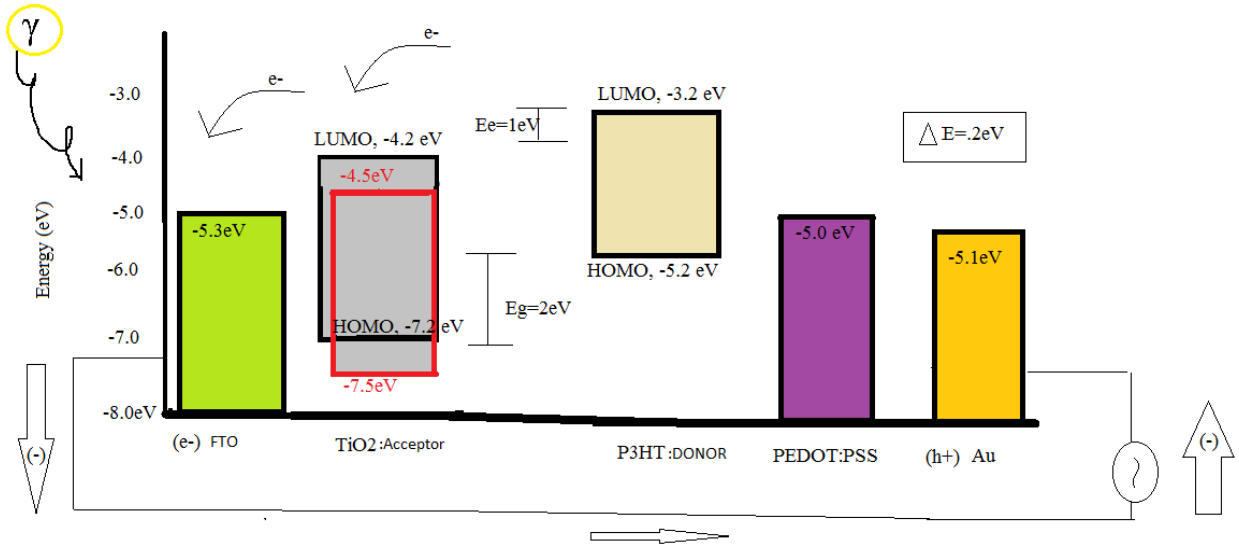

Figure 30: Band gap alignment of a Hybrid polymer-nanoparticle solar cell

and there are a lot of open-source resources on its handling. Once we had narrowed our focus in the materials we wanted to use in our active layer, we then determined suitable other mateirals to use as the electron transporting layer (ETL), hole transporting layer (HTL) and electrodes by finding suitable band-gap alignments that would promote unidirectional flow, with materials that could be deposited using apparatuses to which we had access. We decided to fabricate the following inverted-architecture solar cell in this order: FTO/TiO_2/TiO_2 and P3HT/PEDOT:PSS/Au. This can be seen in Figures 29 and 30.

Experimental Technique

In this report, we assemble several different layers of test cell that are not the same as the ones listed in our theory section, as we had some difficulty assembling a pure TiO_2 layer, and hoped that a more simple cell would be able to function, even if not efficiently, and give us some

idea of how to better proceed. The reason we decided to do this is because we had difficulty coating a thin, homogeneous ETL. As such, there are several different types of cells we assemble at the end of this procedure:

- FTO glass/P3HT and TiO_2 nanoparticles/PEDOT:PSS/Au
- FTO glass/P3HT only/PEDOT:PSS/Au on FTO
- FTO glass/P3HT and TiO_2 nanoparticles/PEDOT:PSS/Au on FTO
- FTO glass/TiO_2/P3HT only/PEDOT:PSS/Au on FTO
- FTO glass/TiO_2/P3HT and nanoparticles/PEDOT:PSS/Au on FTO

The original intended architecture was FTO/TiO_2/P3HT and TiO_2/PEDOT:PSS/AU. This report first summarizes the most successful procedure found to produce a homogenous coat of each layer, then goes through the analysis of each layer (including the unsuccessful TiO_2, and then further attempts to refine it), and how thickness was determined for each.

For testing purposes, we had planned to assemble cells with several different ratios of TiO_2 to P3HT in the active layer. The first will have none, the second will be 1:.5, the second 1:1, and the last 1:1.5. We planned to make two of each, leaving us with a total of 16 cells to test. This was not completed as functional prototypes were never reached.

The things we completed and tested included: Cleaning the FTO glass, three different attempts to make a continuous TiO_2 layer [33][34]. Perfecting and measuring the P3HT layer, Perfecting and measuring the PEDOT:PSS layer, Calibrating the sputter coater to deposit a known amount of Au, and calibrating the spin coater speeds.

Fully assembled cells were made 6 times, and a discussion on how they were tested is included in the following section.

Part I: Procedures

1. Wash FTO substrate (~30 ohms/sq, 25mm × 25mm × 1.1mm, purchased from TechInstro)
    a. Take one substrate and place it face up inside a beaker.
    b. Place the beaker in the fume hood and pour acetone into the beaker to a level above the substrates, so that the substrates are immersed in solvent.
    c. Cover the top of the beaker with a piece of foil.
    d. Place this beaker in the sonicator and sonicate for 10 minutes.
    e. Remove the beaker from the sonicator and dispose the acetone into the waste container. Rinse twice in Di H_2O
    f. Repeat step c, but this time using isopropanol. Pour isopropanol into the beaker to a level above the substrates. Cover with foil and place in sonicator as done previously and sonicate for 10 minutes. Repeat step f.
    g. Repeat step g but this time using Di H_20
    h. Dry on a clean hotplate covered with an upside-down beaker
    i. Immediately after cleaning begin the deposition, or store in an evacuated desiccator in Di H_20.
2. TiO_2 layer Method A

a. Glass cover slips were cleaned according to protocol and dried on a hot plate while covered with another clean glass beaker to prevent contamination
b. 1.0 mg of TiO_2 were dissolved in ~5 ml PEG and stirred overnight on a stir plate
c. 120 microliters of solution were statically deposited onto slides and the meniscus was pulled to the edges
d. Solutions were spun at 2000rpm and 5000rpm for 60s
e. Annealed from 20ºC-250ºC slowly with step intervals over the course of an hour
f. SEM Images and Edax taken of slides. All contain aggregates

3. Alternative TiO2 layer Method B
    a. Solution: .099g TiO_2 with 3 ml PEG and 2 ml 10% HCl
    b. Sonicated and left on stir plate overnight, then sonicated again
    c. Statically deposited 120 microns onto a clean slide at 2000 and 5000rpm for 60s
    d. Annealed slowly from 50ºC-230ºC in step intervals
    e. Still had aggregates
4. Alternative TiO_2 Method C
    a. Solaronix Precursor(Ti-Nanoxide T-L/SC)
    b. Dynamically dispensed 40 microns onto a clean slide at 4,00 rpm for 30s
    c. Annealed slowly from 50-200ºC with step intervals over the course of an hour
5. Prepare Active Layer-All layers were confirmed by eye to be homogeneous after spinning (No holes or obvious streaks). Any slides with imperfections were disposed of and not used.
    a. No TiO_2
        i. Dissolve 20 mg/ml of P3HT in xylene in an amber vial (100 mg/5 ml)
        ii. Place vial on hot plate (70°C) with a stirrer bar for 30 minutes; then sonicate
        iii. Filter with a 0.45 µm PTFE filter
        iv. Pipette 20 µl of the above solutions onto a substrate spinning at 2000 rpm and spin for 30s+6s to allow time to dynamically deposit
        v. Thermally anneal at 100°C for 10 minutes.
    b. TiO_2
        i. Dissolve 20 mg/ml of P3HT in xylene in an amber vial (100 mg/5 ml)
        ii. Place vial on hot plate (70°C) with a stirrer bar for 30 minutes; then sonicate
        iii. Filter with a 0.45 µm PTFE filter
        iv. Add in TiO_2 in concentrations of 1:1, 1:2, or 1:3
        v. Sonicate for 10min (water in beaker should be hot)
        vi. Leave on stir plate for 3hrs
        vii. Sonicate again for 10min (water in beaker should be hot)
        viii. Pipette 20 µl of the above solutions onto a substrate spinning at 2000 rpm for 30s+6s to dynamically deposit
        ix. Thermally anneal at 100°C for 10 minutes.

6. PEDOT:PSS
    a. Filter PEDOT:PSS solution through the 0.45um PVDF filter into an amber vial
    b. Preheat the hot plate to 150°C
    c. Place a freshly prepared substrate into the spin coater and coat at high speed (5000-6000 rpm) for 30s
    d. After spinning has completed visually inspect the PEDOT:PSS films for defects and for best performance discard any substrates with imperfections.
    e. Anneal on the hotplate for 5 min at 150°C then store immediately in evacuated dessicator or immediately deposit anode
7. Sputter coat on gold anode
    a. Mask the area wished to be used as a cathode on the back electrode with tape to ensure there are no shorts, being sure to extend the tape to cover a thin strip of the active material
    b. Using a sputter coater, deposit around 100nm of gold using sputter coater for 23min
8. Attach connections
    a. Using a silver-loaded glue, attach several wires directly to the gold anode. Allow to dry in an evacuated desiccator over night

Part 2: Characterizing the layers

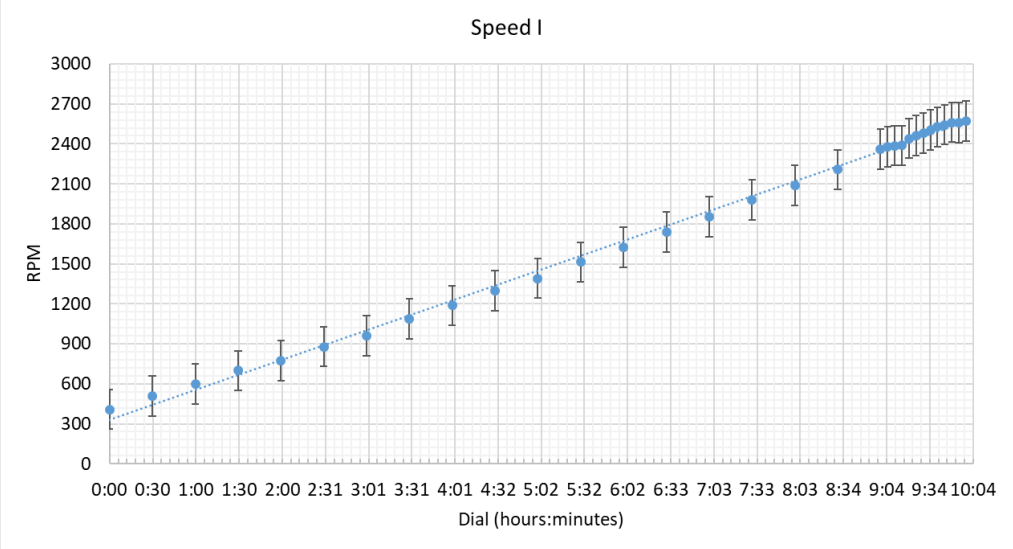

Figure 31: Calibration curve for the spin coater: Fine adjustment.

Deposition of all our layers were done with a KW-4A Spin Coater (110V). The spin coater was recalibrated by hand using a Monarch instrument PLS pocket LED strobe. Calibration curves were then added to the official handbook for future students to use and are included in figure 31 and 32. A great review on spin coater theory was written by Ossila[35].

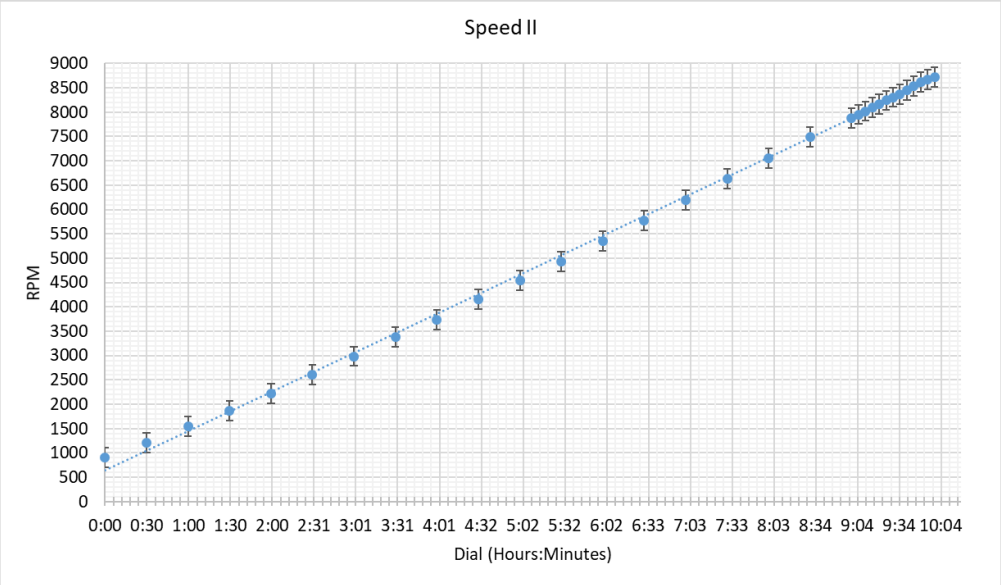

Figure 32: Calibration curve for the spin coater: Coarse adjustment.

1. TiO_2 Method A and B, and Method C:

TiO_2 layers spun on clean glass cover slips were examined under the HighRox to view the aggregates and measure the size of the particulates. Particulates ranged in size from >10nm to well over 50nm. After adding HCl to the mixture the particles may have decreased in size and number, although not significantly. A picture of the aggregates taken on the SEM can be viewed in figure 33.

To determine whether or not there was a thin layer of TiO_2 in between the aggregates, the slides were viewed on a slanted mounted in the PHENOM. An EDX was taken of the aggregates, the area between the aggregates, and of plain glass. The plain glass slide gave a concentration of Ti that was .4 $\pm$ .9. EDX over the TiO_2 aggregate gave a Ti concentration of 5.1 $\pm$1, and the area in between the aggregates gives a concentration of 1.5 $\pm$1. This indicates there is some faint traces of TiO_2 in between the larger aggregates, and there may in fact be a thin layer of continuous thin film in between the aggregates. As seen in the angled SEM image taken of the side of the slide (Figure 34), there is some sort of film that is different than the glass slide along the edges of the slide.

Attempts were made to measure the thickness via ellipsometer, and DEKTAK but were eventually abandoned due to the fact that inconsistency in the homogeneity of the layer did not allow us to get an accurate reading. Method C was analyzed using the filmetrics surface profilometer once it was up and running; however, it also could not get an accurate reading due to the transparency of the layer.

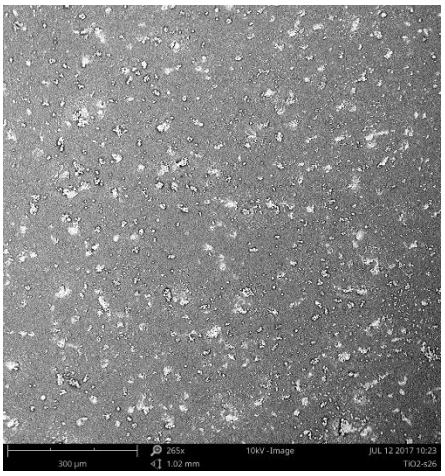

Figure 33: TiO_2 coated slide taken on PHENOM

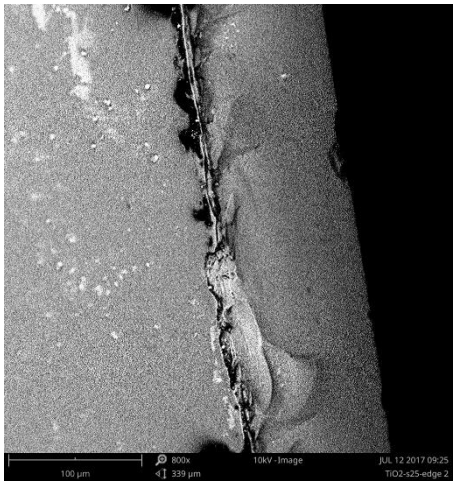

Figure 34: Edge of TiO_2 coated slide taken on PHENOM

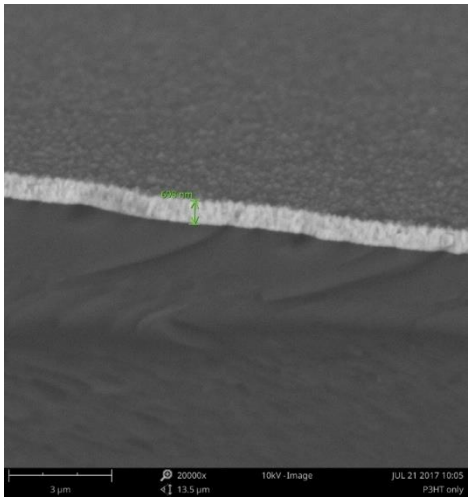

Figure 35: P3HT coated FTO on Phenom. 75 degree angle

2. P3HT

Attempts were made to measure the thickness via the DEKTAK but were eventually abandoned as attempts to mask the slides inadvertently altered the thickness of the layer. Eventually, a procedure was developed to test the thickness of the layer using a PHENOM (a type of SEM) First, an FTO slide was coated via the procedure above, then the slide was turned upside down with the part that was not going to be viewed resting against a plastic ruler. One corner was gently scored using a diamond stylus and broken off by lining up the diamond cutter in the score and hitting it sharply once. The corner was then mounted on a stud that had a 75 degree angle, with the smooth edge aligned in line with the top of the stud. Images were taken and measured on the PHENOM and can be seen in figure 34, this is of course a horizontal the projection. A quick recalculation to account for the angle of the slide gives a thickness of about 698*Cos(75)=180nm.

3. PEDOT:PSS

The PEDOT:PSS was measured with the same procedure above using the PHENOM and found to be around 173nm.

4. Calibrating the Gold layer

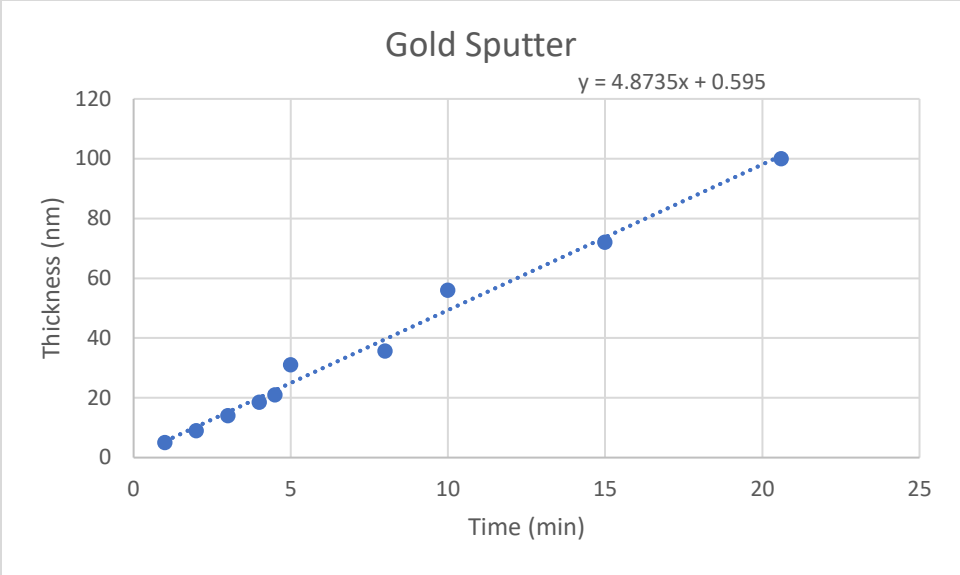

Figure 36: Gold Sputter Coater Calibration, measured by masking slides and sputtering for different increments, then measuring the thickness using a DEKTAK

The gold is to be sputtered on. The thickness of a sputtered layer is directly proportional to the time spent sputtering. There was a calibration curve for gold that came with the HUMMER; however, we were skeptical as to whether this would match up with our target. As such, the sputter coater was re-calibrated by sputtering several masked glass slides at different times (3s, 5s, 8s, 10s, and 15s). Thickness of each was measured using the DEKTAK and graphed (Figure 36). A linear trendline was added, and after confirming it matched the existing trendline for gold in our hummer, the two lines were combined and projected out to give the time needed to get about a 100nm thick layer of gold to be ~23min.

Part 3: Full assembly, including connectors and future procedures

After assembling each of the layers in one of the ways as seen above copper wires were attached to the top using silver-loaded glue. If TiO_2 nanoparticles were used in the active layer they were incorporated at a ratio of 1:1.5 for the active layer.

Example images of fully assembled cell can be seen in figure 37. Cells were tested under a single LED bulb (110V, 4W, GU10 LED Bulbs - 6000K Daylight Spotlight - 330 Lumen) at 123616 Lux. Problems encountered included:

- Difficulty getting the PEDOT:PSS to spin on top of the P3HT. The solution to this problem involved statically dispensing the PEDOT:PSS and drawing the meniscus to the edge using the tip of the pipette.
- Potential shorting when sputtering on the back anode. Solutions found involved both masking the bottom layer before sputtering, and leaving a significant portion uncovered to be absolutely sure no shorts occurred (see the top image in figure 36, a thin line of purple can be seen on the left of the gold layer), or sputtering a

Figure 37: An example of a complete assembly. Top image shows the back of the cell, with the gold back-electrode. Bottom image shows the top of the cell where light would enter. Note: The streaks came from the spin coater on the back side of the glass, and are not due to inhomogeneity in the layer

separate piece of conductive glass and pressing the two together. This method was not preferred as it inevitable was likely to have connection issues.

- Once deposited the active layer quickly begins to degrade, and in addition they were very sensitive to fluctuating temperatures and excessive humidity. In addition, the sputter coater is located across campus from the fumehood where the spin coater was located. An evacuated glass, portable dessicator was used to transport the cells; however there is no guarantee that this did not open up the potential for the cells to degrade in the process of transportation.

- The silver glue used as a connection may have had a solvent which was degrading the layers and causing additional short problems. This was not tested; however is something to be aware of if later assemblies are to be attempted.

A voltmeter was used to measure the voltage and current through the cell by gently pressing one probe to the top of the cell, and gently holding the other on the copper strips attached to the anode. 0V were read and 0mA. This was also repeated outside at approximately 1 kW/m^2, and 0V were read and 0mA.

Results were repeated using a picoameter, the GAMRY, to test for diode action as discussed in the above section 3.5. Rectification was never seen in any of our fully assembled cells. We then tested each of our individual layers versus a P or N doped silicon wafer for diode-like behavior, to see whether the problem was with any of individual deposition methods. Five slides were made. Two with TiO_2 only, Two with PEDOT:PSS only. The tests ran were: P vs TiO_2, N vs TiO_2, P vs PEDOT:PSS, N vs PEDOT:PSS. Tests were run using the Solaronix precursor for the TiO_2 layer. As can be seen in figure 38, a large rectification is seen when the TiO_2 is placed against the N-doped layer, and a large rectification can be seen when the PEDOT:PSS is placed against the P-doped layer; however, no rectification is seen between the TiO_2 and PEDOT:PSS.

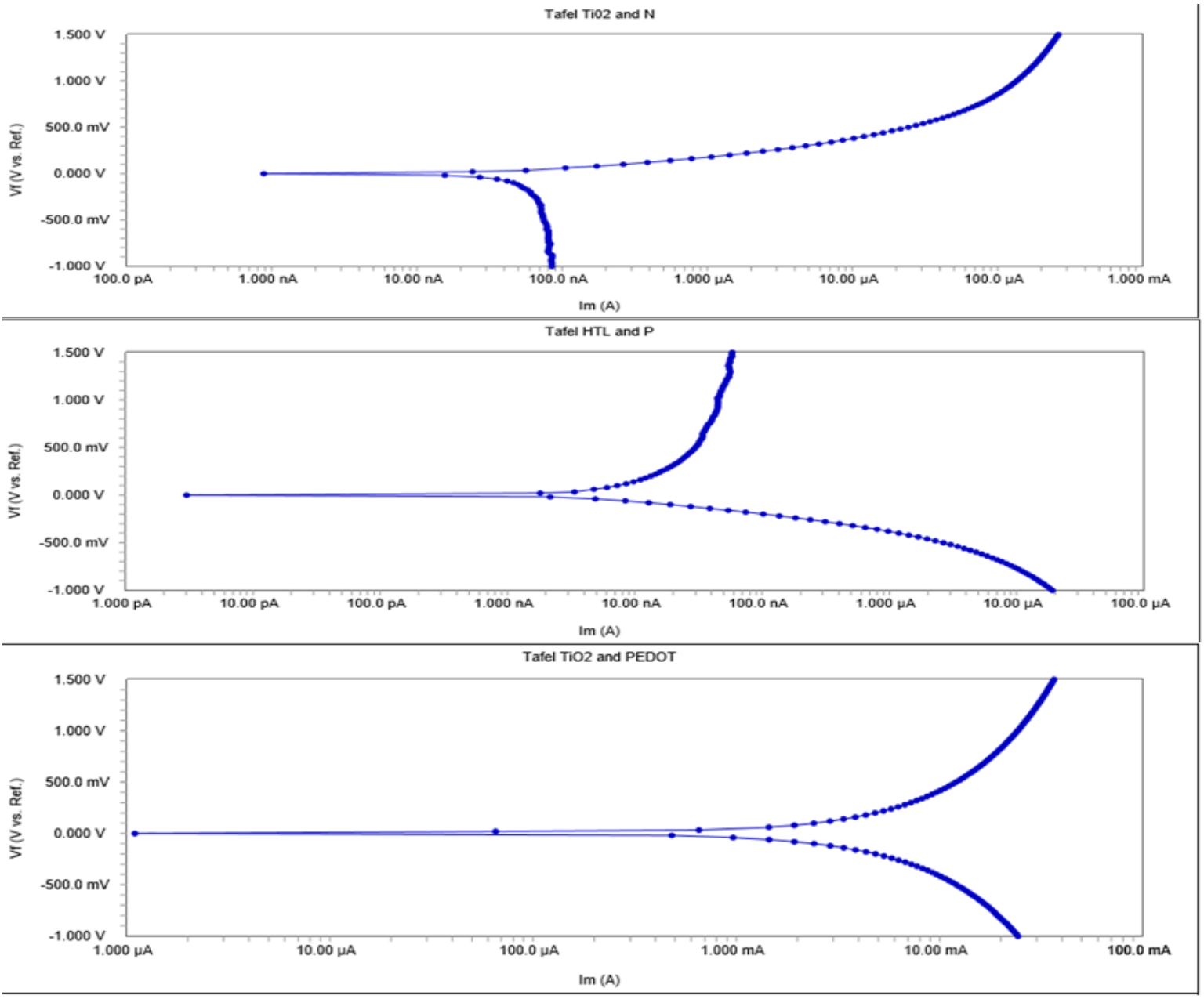

Figure 38: Top: TiO_2 layer against an N-doped silicon wafer showing clear rectification in the negative direction. Middle: PEDOT:PSS against a p-doped silicon wafer showing clear rectification in the positive direction. Bottom: TiO_2 vs PEDOT:PSS not showing any significant rectification

This was a concerning realization that indicates why our assembled cells are not working; however, literature searches could not reveal a plausible explanation for this problem, and in the interest of time for the completion of this thesis, it was decided that this type of cell was not preferable for testing our diatoms. Despite this, much potential still remains for futrue research in this area, if this lack of diode-action between the two layers couldbe corrected.